Key Points:
- Simulations reveal significant alterations in surface water source patterns in a wetland floodplain due to projected climate change by 2099.
- Different climate scenarios have variable and sometimes counterintuitive impacts on water source patterns.
- Spatial analysis of the water sources trend in the floodplain shows greater sensitivity to climate change than lumped model output.

Impact of Climate Change on Water Sources and River-Floodplain Mixing in the Natural Wetland Floodplain of Biebrza River

Tomasz Berezowski[1] and **Daniel Partington[2]**

[1]Faculty of Electronics, Telecommunications and Informatics, Gdansk University of Technology, Gdansk, Poland, [2]National Centre for Groundwater Research & Training (NCGRT), College of Science & Engineering, Flinders University, Adelaide, SA, Australia

Abstract The origins of river and floodplain waters (groundwater, rainfall, and snowmelt) and their extent during overbank flow events strongly impact ecological processes such as denitrification and vegetation development. However, the long-term sensitivity of floodplain water signatures to climate change remains elusive. We examined how the integrated hydrological model HydroGeoSphere and the Hydraulic Mixing-Cell method could help us understand the long-term impact of climate change on water signatures and their spatial distribution in the protected Biebrza River Catchment in northeastern Poland. Our model relied on 20th century Reanalysis Data from 1881 to 2015 and an ensemble of EURO-CORDEX simulations for representative concentration pathways (RCP) 2.6, 4.5, and 8.5 from 2006 to 2099. The historical component of the simulations was subjected to extensive multiple-variable validation from 1881 to 2019. The results show that the extents of water sources were rather stable in the floodplain in the 1881–2015 period. The projected future impacts were variable with each analyzed RCP, but in all cases, different significant trends were present for the spatial distribution of water sources and for the river-floodplain mixing. However, the total volume of water from different sources was less sensitive to climate change than the dominant sources and spatial distribution of water. The simulation results highlight the impact of climate change on the extent of water sources in temperate zone wetlands with significant implications for ecological processes and management. These results also underscore the urgent need to leverage such modeling studies to inform protective and preservation strategies of floodplain wetlands.

Plain Language Summary In this study, we used a hydrological model that was capable to simulate volumes of water from rain, snowmelt, groundwater discharge, and river flooding to investigate how these volumes will vary with the climatic conditions. For the study site, we selected the Biebrza River wetland floodplain, where former research highlighted the presence of these water sources in inundation during flooding. It was also known that the water sources have different chemical (e.g., nutrients) and physical (e.g., sediments) compositions and they correlate with the vegetation in the wetland. Hence, any change in the extent of these water sources (driven e.g., by climate change) may affect vegetation. Our research indicated that indeed the spatial extent of water sources will strongly vary with the future climate projection while the less detailed floodplain-wise volume of the water sources will not vary that much. We also showed that the direction of change in the water sources' extent will be different given the analyzed climate scenario. These results should be taken into account especially by the natural conservation managers to prepare for the changes.

1. Introduction

Mixing of river and floodplain water during floods, also known as perirheic mixing (Mertes, 1997), has great significance for ecological and hydrochemical processes. This significance in floodplain ecology is reflected by the floodplain vegetation zonation, which is related to the differences in the chemical or sediment composition of water from river and groundwater, rain and snowmelt inundation in the floodplain (Chormański et al., 2011; Keizer et al., 2014). Similar relations are present in the Amazon floodplain, where the mixing of sediment-rich and sediment-poor water near the confluences is related to vegetation (Park & Latrubesse, 2015), and avifauna (Laranjeiras et al., 2021). Also, in the Amazon floodplain, the river-floodplain water frontier is controlling the crevasse splays occurrence (Aalto et al., 2003). The hydrochemical significance of water mixing is mainly due to nitrate removal by denitrification. This process occurs in the flow-through wetlands, where nitrate- and

oxygen-rich water from a river mixes with the oxygen-poor floodplain water. Although this effect was reported in several floodplains, including Atchafalaya (Jones et al., 2014; Scott et al., 2014), Po (Racchetti et al., 2011), and Wisconsin (Forshay & Stanley, 2005), to achieve considerable nitrate removal a significant floodplain area has be connected to the river (Natho et al., 2020). As we have shown previously for a natural temperate zone wetland floodplain - Biebrza River, the river-floodplain water mixing, or the active perirheic zone, is very dynamic in space and time (Berezowski et al., 2019). In that study, we used state-of-the-art modeling tools for a single flood event study, hence we were not able to assess the active perirheic zone's long-term variability and the role of the changing climate.

Hydrological impact models of climate change predict a shift of the highest and lowest discharges at the end of the twenty-first century for several regions of the world (Arnell & Gosling, 2016; Giuntoli et al., 2015; Prudhomme et al., 2013). These regions include the major floodplain and wetlands, where the shift in flooding pattern may influence ecological processes such as vegetation development (Garris et al., 2014; Murray-Hudson et al., 2006; Thompson et al., 2016; Zulkafli et al., 2016). The hydrological shifts in the future will also lead to changes in floodplain connectivity in unregulated floodplains. This may result in increased nitrate removal by denitrification, as simulated for the Lower Missouri River (Jacobson et al., 2022). Nitrate removal varies in floodplain habitats with different contact with river water (Scaroni et al., 2011). Since, the zonation of water sources within the flooding extent is relevant for vegetation development and denitrification, more precise quantification of these ecological processes in the scope of climate change could be achieved by analyzing water sources' zonation. This remains a gap in the literature.

Modeling of climate change impact on floodplain inundation is usually done using either 1D or 2D hydrodynamic models in which the surface water in the floodplain lacks or has limited feedback with parts of the catchment that are not represented by the hydrodynamic model. These feedbacks are important in the proper modeling of floodplain inundation, as those minor water sources produce the inundation in remote parts of the floodplain and determine the river-floodplain water frontier (Berezowski et al., 2019) and groundwater mixing zone (Nogueira et al., 2022). Therefore, to achieve full feedback between all water sources integrated hydrological models (IHMs) are required (Sebben et al., 2013). The computational complexity of these models often requires some simplifications or limiting the simulation area (Barthel & Banzhaf, 2015) to achieve feasible run times. Also, the application of IHMs to climate change impact research is limited in scenarios and analysis periods lengths (e.g., Erler et al., 2019; Ferguson & Maxwell, 2010; Sulis et al., 2011). On the other hand, using a general circulation models (GCM) ensemble reduces uncertainty related to future climate projections impact on hydrology (Kundzewicz et al., 2018). Currently, this research area remains relatively unexplored, as only a few studies run IHMs with long-term forcing data from GCMs ensembles, such as the Intergovernmental Panel on Climate Change emission scenarios (Boko et al., 2020; Goderniaux et al., 2009; Perra et al., 2018; Ramteke et al., 2020; Sulis et al., 2012; Yuan et al., 2021) and no IHMs have analyzed the extent of water from different sources.

To examine the impact of climate change on spatiotemporal water signatures during flooding in a natural temperate zone wetlands, this research aims to employ a robust IHM for the Bierbza catchment to investigate the long-term variability of the extent and mixing of water from different sources during flooding. The model for the Biebrza will be run for a historical period using 20th Century Reanalysis data and a GCM ensemble for representative concentration pathways (RCP, which describe climate scenarios based on emission levels) 2.6, 4.5, and 8.5 scenarios for the future. With this model, the aims of the research are:

- To determine if the past climate and future climates under RCPs 2.6, 4.5, and 8.5 will drive any significant changes in the spatial distribution and dominance of water sources in the Biebrza floodplain.
- To determine if the volume of water in the floodplain will significantly change under past climate and possible future climates with RCPs 2.6, 4.5, and 8.5.

Finally, we highlight the implications for ecological processes, modeling, and management strategies under climate change.

2. Methods

2.1. Study Area

The Biebrza catchment (22.7°E, 53.7°N) is of medium size, 7,091 km^2 and the lower Biebrza valley (hereinafter referred to as floodplain), where we focus our analysis comprises 297 km^2 (Figure 1).
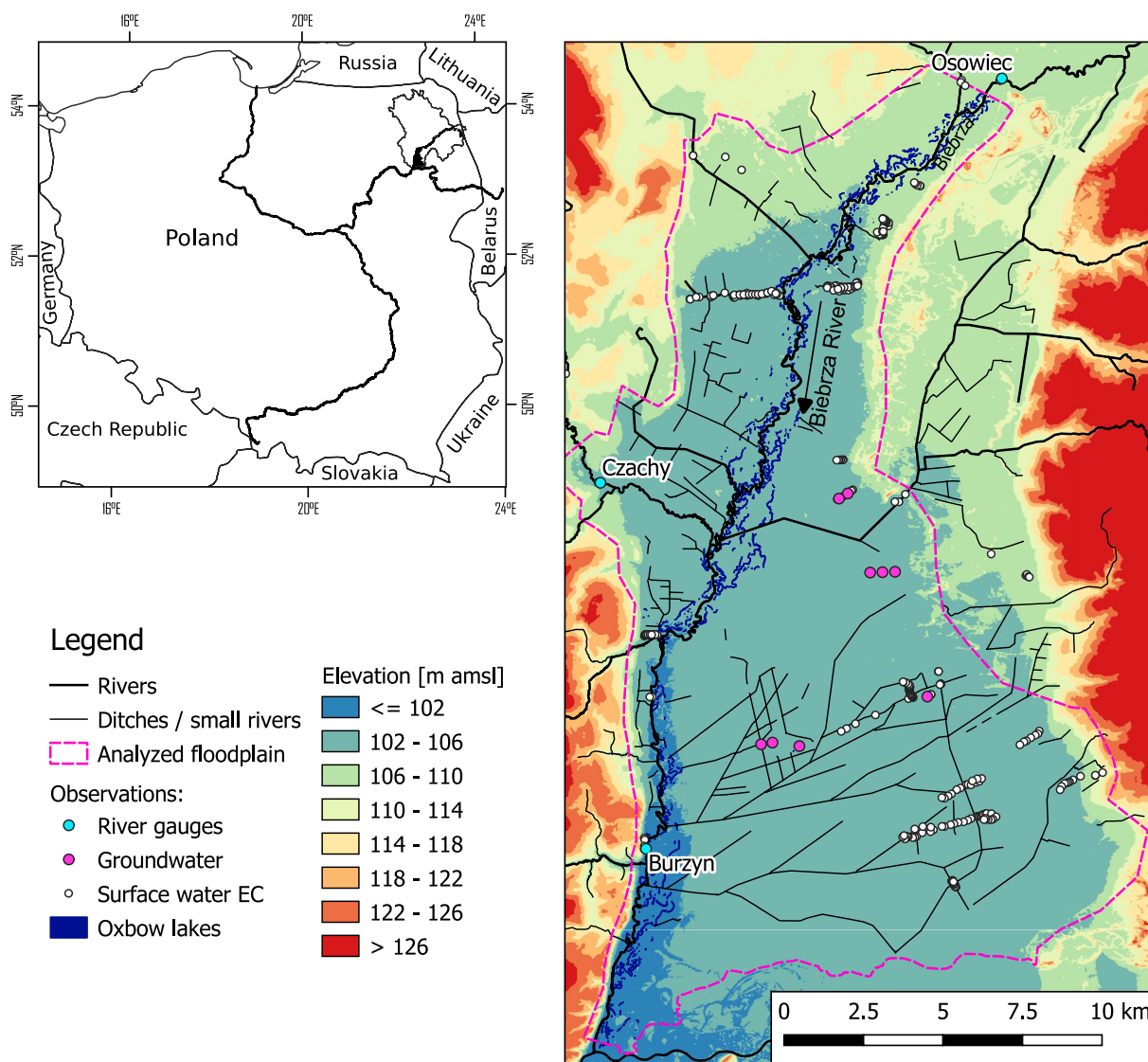
Figure 1. The floodplain area and the measurement points (right panel). Location of the study area in Poland (left panel) with the major rivers (blue lines), Biebrza river catchment (black outline), and the floodplain (black patch). The legend concern only the right panel.

The major river engineering work was conducted in the area in the first half of the 19th century to establish a waterway between Biebrza and Neman Rivers. Next, in the middle of the 19th century parts of the wetlands located in the lower and middle parts of the valley were meliorated. Since then, human impact in the floodplain area was low, although some melioration work was conducted in the upstream parts of the catchment (Banaszuk, 2004). Currently, the anthropogenic pressure is low, as the population density in the region where the Biebrza River catchment is located is the lowest in Poland (58 people per km^2) (Statistics Poland, 2021). The future population projections for this region predict a 32% decline between 2020 and 2100 (Eurostat, 2019). The Biebrza valley was grazed and mowed in the past and aquatic vegetation in the river was occasionally removed (Berezowski et al., 2018). Since the establishment of the Biebrza National Park in 1993 mowing and grazing is continued as an active protection measure (Kotowski et al., 2013). Currently, the Biebrza National Park is one of the largest active protection areas in Europe (59,223 ha), with the Biebrza Wetlands listed as Ramsar and Natura 2,000 sites.

Long-term average daily discharge in Biebrza River for the Burzyn gauging station (Figure 1) has been 38.1 $m^3 s^{-1}$ (1970–2005), with a minimum of 4.33 $m^3 s^{-1}$, maximum of 517 $m^3 s^{-1}$, and 99th percentile of 173 $m^3 s^{-1}$. Daily water level ranges from 99.84 to 103.81 m above mean sea level (AMSL) with the 99th percentile of 102.54 m

AMSL and the bankfull level of 101.31 m AMSL. The river flooding area reaches up to 52.5 km^2 and inundation can last on average between 121 and 193 days per year depending on location (Grygoruk et al., 2021), which is considerably longer than for typical temperate zone rivers. The total flooding extent due to all water sources was not assessed by modeling for longer time periods, however, the field observations show that almost the entire area of the floodplain is inundated with shallow water from rain, snowmelt, or groundwater (Chormański et al., 2011). Model simulation carried out for the 1-year period shows, that river and floodplain water interact after the river water levels are above bankfull (which corresponds to about 33 m^3 s^{-1}), but the zone strongly varies during flood development (Berezowski et al., 2019). The average annual precipitation over the period 1970–2005 in the catchment has been 672 mm (DJF = 126 mm, MAM = 143 mm, JJA = 236 mm, SON = 167 mm), of which 88 mm was snow, the mean daily temperature was 7°C (DJF = −2.7°C, MAM = 6.8°C, JJA = 16.6°C, SON = 7.2°C), and the yearly potential evapotranspiration (PET) was 621 mm.

The hydrogeology of the catchment was considered in the Quaternary deposits, which are 130–212 m deep and the majority consist of glacial till with minor sand layers deposited during the Riss glaciation. Middle and lower parts of the Biebrza valley have a sand layer deposited during the Weichselian glaciation on top of which the Holocene sand and peat layers are present (Banaszuk, 2004). In an about 900 m band along the river channel, numerous paleochannels are present (Figure 1). These are cut-off river meanders developed in the Holocene, that are currently either oxbow lakes or local depressions inundated only during high water levels. The connectivity of the oxbow lakes to the main river affects the microorganisms and fish ecology (Glińska-Lewczuk et al., 2016; Grabowska et al., 2014; Lew et al., 2016).

Wetland vegetation in the floodplain exhibits zonation related to flooding (Pałczyński, 1984). The reeds (Phragmition) belt is located around the river up to about 500–900 m, further away up to 2,500 m from the river, high sedges (Magnocaricion) vegetation is present, and further again, sedge-moss (or fen) vegetation, such as Calamagrostion neglectae, Caricion diandrae, or Caricion demissae is located up to the valley margin.

The vegetation pattern in the floodplain is an interesting feature that was recently analyzed not only in the scope of inundation frequency but also in the scope of the flooding water source (Chormański et al., 2011) and related to the sedimentation pattern (Keizer et al., 2018). Relationship between water sources in inundation with ecological processes have been reported in several world floodplains (e.g., Jones et al., 2014; Laranjeiras et al., 2021; Park & Latrubesse, 2015; Racchetti et al., 2011). Biebrza Floodplain is a suitable site to investigate the impact of climate on water mixing, not only due to its natural character and low human impact but also because it is considered a reference site for similar fen wetlands (Wassen et al., 2006). Therefore, the results of this study will highlight potential climate impacts in similar sites.

2.2. Forcing Data

Hydrological simulations for over two hundred years period required several sources of forcing data for the IHM, that included air temperature, rain and snow precipitation, and potential evapotranspitarion (Table S1 in Supporting Information S1). The criteria for selecting a data source were daily (or higher) temporal resolution and availability of the required forcing variables. The historical and future climate data biases were corrected using the quantile mapping (Gudmundsson et al., 2012) method. The details of forcing data processing, bias correction application, their results and discussion are presented in Text S1 in Supporting Information S1.

For the historical 1880–2015 period we used the 20th century climate reanalysis (20CR) data in 1° × 1° resolution (Slivinski et al., 2019). We used ensemble mean (80-member ensemble) from this data set as our analysis showed that int matched the meteorological observations for the same period.

For the future period, we used the EURO-CORDEX data (Jacob et al., 2014) from 10 simulations using different GCMs (Table S1 in Supporting Information S1). Each simulation used the SMHI-RCA4 regional climate model. We selected all available simulations from the EURO-CORDEX archive that had the required forcing data for the hydrological model. Only five out of 10 simulations had the required forcing data for RCP 2.6. To investigate the effect of greenhouse gases emission scenarios on water sources mixing in the floodplain we used the following RCPs: RCP 2.6, which aims to limit the increase in global mean temperature to 2 K by a CO_2 emission decline since 2020, RCP 4.5 which is an intermediate scenario, where the emissions start to decline after 2040, and RCP 8.5 which is a highest emission scenario in which emissions continue to rise during the entire 21st century.

For the 2015–2019 period (for which the 20CR data was not available), when the hydrochemical validation took place, we used the gridded precipitation and temperature data set (Piniewski et al., 2021) and snowfall and snow
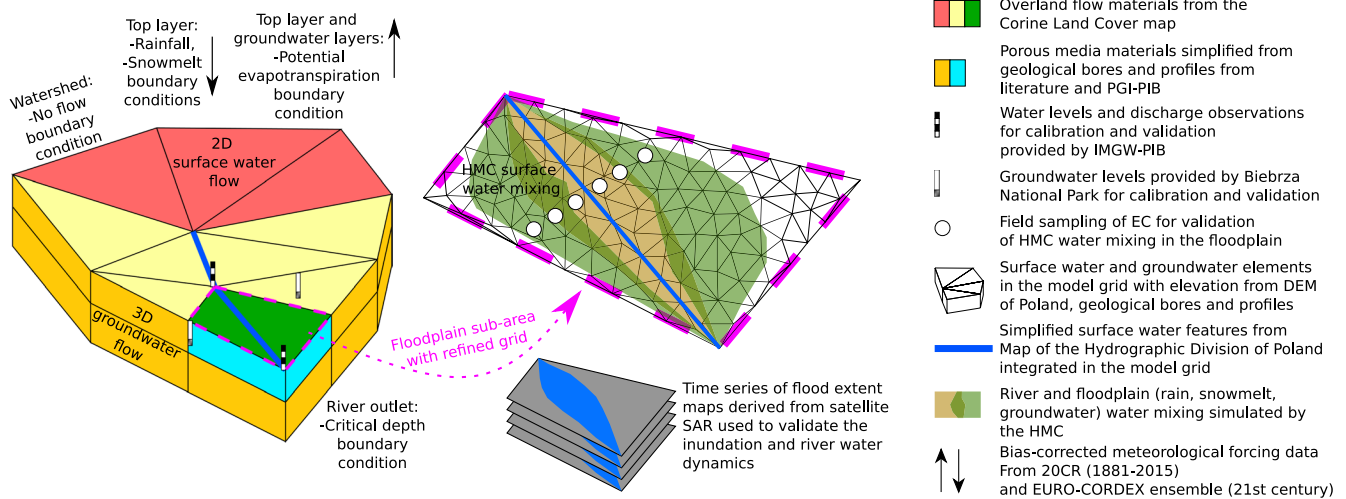
Figure 2. The conceptual representation of the integrated hydrological model used in this study for the Biebrza catchment.

depth data from the Biebrza-Pieńczykówek meteorological station managed by the Institute of Meteorology and Water Management—National Research Institute (IMGW-PIB).

To decrease the data storage from multiple RCPs, EURO-CORDEX models and historical observations in the 219 years period in daily resolution we calculated the daily average value of forcing data variable over all grid cells in the Biebrza catchment and used this data to force the hydrological simulations. This was also justified by the fact that within the floodplain sub area ($\sim 30 \times 15$ km) we did not expect daily precipitation variability that could affect the inundation patterns analyzed in this study.

2.3. Hydrological Model

We simulated the transient water fluxes in the Biebrza River catchment using HydroGeoSphere (Brunner & Simmons, 2012; Hwang et al., 2014) IHM. The 3D groundwater flow was solved using Richard's equation in prism elements and the 2D surface water flow was solved using the diffusion wave approximation of the Saint-Venant equations in triangular elements. The surface-subsurface flow coupling was realized using the first-order exchange. Evapotranspiration flux was simulated using the Kristensen and Jensen (1975) conceptual model, which takes into account interception storage, time-variable leaf area index (LAI), pounding, and soil saturation. Snowmelt and rainfall fluxes were provided as forcing data boundary conditions. The conceptual schematic of the IHM used in this study is presented in Figure 2.

We simulated water mixing using the hydraulic mixing-cell (HMC) method (Partington et al., 2011). In our case the mixing was simulated only for the surface flow domain, however, simulations in groundwater are also possible (Nogueira et al., 2022). The HMC method accounts for water fluxes from various boundary conditions and groundwater discharge effectively producing a fraction of each water source in a model node. Water sources were differentiated spatially. To calculate the river water fractions we summed inflow of all water from upstream of the floodplain area. Whereas in the floodplain area, original fractions of rainfall, snowmelt, and groundwater were used to represent the inundation components generated therein. In the first time step, the fractions are initialized using an artificial initial fraction, equal to one.

The HydroGeoSphere model uses LAI during the estimation of evapotranspiration. Since LAI was not available in any data set covering the simulation period we used a degree-day model to simulate LAI for each meteorological data set used in this study (Text S2 in Supporting Information S1).

2.4. Model Grid

To prepare the model grid we processed the relevant geographical information as detailed in Text S3 in Supporting Information S1. To conduct the IHM simulations for the 7,000 km² catchment we simplified the geometry

of the rivers by limiting the minimum node distance to 125 m along the river course for major rivers and 500 m for minor rivers. For the major rivers, the banks were limited to a 60 m buffer around the river. This forced the perpendicular river cross-section to be trapezoidal. For minor rivers, no buffer was created and the perpendicular cross-section was triangular.

The river nodes, wells locations, lakes, oxbow lakes, and the catchment boundary were used to generate a Delaunay triangular grid with the "triangle" software (Shewchuk, 1996). We refined the grid fourfold in the floodplain area and relaxed the nodes using an algorithm provided by Kaser et al. (2014). The grid refinement allowed to simulate better the hydrodynamics of the floodplain, preserve lager oxbow lakes, and preserve morphology of larger river features. The triangular grid consisted of 19,297 nodes and 38,081 elements of which 10,436 were in the floodplain. The overland flow materials were distributed spatially according to the Corine Land Cover map (Commission of the European Communities, 2013) and the surface elevation was set based on the Digital Elevation Model (DEM) of Poland in the resolution of 1 m (Figure S4 in Supporting Information S1).

Vertically the grid consisted of six layers with three porous media materials: glacial till, sand, and peat (Figure S5 in Supporting Information S1) distributed according to geological cross-sections (Banaszuk, 2004) and bore profiles (Polish Geological Institute, 2014). In total, the 3D grid consisted of 135,079 nodes and 228,486 prism elements.

2.5. Error Metrics

In this study, we use the same error metrics for a number of different simulated quantities, such as water levels, discharge, water source fractions, and area. We present the general form of the equations below. Whenever a given error metric is used in the text it is specified based on which quantities it was calculated for and, if applicable, to which quantity it was normalized.

The Kling-Gupta efficiency [-]:

$$\text{KGE} = \sqrt{(r-1)^2 + (\alpha-1)^2 + (\beta-1)^2} \tag{1}$$

where r [-] is the correlation coefficient between simulated and observed quantities, α [-] and β [-] are ratios of simulated to observed quantities mean and standard deviation respectively. The KGE ranges between $-\infty$ and 1 and the higher the value the better fit to the observation is achieved by the model.

The root mean square error [units the same as input data]:

$$\text{RMSE} = \sqrt{\frac{\sum_{i=1}^{N} \left(\hat{h}_i - h_i\right)^2}{N}} \tag{2}$$

where h_i and $\hat{h}_i$ are observed and simulated quantities respectively for a data record (e.g., time step) i out of N. The RMSE represents the magnitude of error between the observations and simulations and ranges between 0 and ∞.

The systematic error, or bias [units the same as input data]:

$$b = \sum_{i=1}^{N} \hat{h}_i - h_i \tag{3}$$

where the symbols are the same as in Equation 2. The bias shows whether the simulated quantities overestimate (positive b) or underestimate (negative b) the observed quantities and $b = 0$ indicate no bias.

The linear correlation between two variables was quantified using Pearson's correlation coefficient (r) [-] and the fraction of variance explained between the two variables was quantified using the coefficient of determination (r^2). If two variables are time-dependent the linear correlation can be interpreted in terms of the temporal variability agreement between them.

2.6. Model Calibration

We used a screening approach to find an optimal parameter set for the hydrological model. For this purpose, we randomly sampled 800 random parameter sets using the Latin hypercube algorithm using the "tgp" *R*

package (Gramacy & Taddy, 2010). Each set consisted of 26 unique parameters, which were fuhrer transformed to produced correlated parameters (e.g., different water-retention parameters) as explained in Table S5–S7 in Supporting Information S1). The calibration period was 2 years and 10 months (2004-01-01 to 2006-10-31) followed by a one and half year warm-up period (2002-06-01 to 2003-12-31). This period was chosen because it represented well the historical variability of hydrological conditions. The initial conditions for each calibration run were transferred from a steady-state simulation using parameters from our previous model version (Berezowski et al., 2019).

We choose the best model base on KGE for two discharge stations and RMSE [m] for five groundwater wells heads. The locations of discharge stations were chosen at the inlet and outlet of the floodplain (Osowiec and Burzyn) and the location of the wells were chosen two in the floodplain, one in the middle and upper parts of the valley. The relation between average KGE and average RMSE for all stations forms a Pareto front with a group of the best parameter sets from which the final model was selected manually by reviewing the simulated hydrographs.

2.7. Model Validation

2.7.1. Hydrological Validation

We used several contemporary and archival data sources with varied temporal coverage for the validation of simulated river flow and groundwater heads (Table S4 in Supporting Information S1). We used the same error metrics as for calibration and the RMSE was normalized by the data range for each station or well.

The most of the river water level records before 1950 (Table S4 in Supporting Information S1) contained only the relative water level in reference to the gauge zero level. For these records we calculated the absolute water level, that is, in meters AMSL, using a relation between the mean value of absolute and relative water levels for the remaining records for a particular gauge. The disadvantage of this approach is that the temporal trend is not preserved and the RMSE and systematic error are biased.

Some of the groundwater heads data were missing the absolute readings, that is, depth instead of elevation was measured. Calculation of the absolute levels was done by using a 1×1 m DEM values in the well location as the zero depth. Few groundwater wells showed a clear step in the records, which could have been due to the displacement of the reference point. We removed records with the step from the database.

2.7.2. Remote Sensing Validation

We validated the simulated water extent using a multi-temporal remote sensing data set (Berezowski et al., 2020). In that data set 161 water extent maps were developed for the 2014–2019 period using the Sentinel-1 synthetic aperture radar (SAR) for the floodplain. The average water level error of the SAR flood extent maps was 0.21 m. The major drawback of this data set was that in densely vegetated areas the flood extent was obscured and effectively these areas are labeled as not flooded even if the water level was high. Further, the data set was not sensitive to shallow water, which limits its applicability only to an indication of deeper river water within the Biebrza flooding extent. Despite the drawbacks, the remote sensing data set was a good indicator of the temporal dynamics of the flooding extent, especially for the river water zone. From this data set, we selected 134 flood maps with the lowest error and used them along with the hydrological model output to calculate validation metrics.

The remote sensing validation in the floodplain was calculated using the total flooding area due to simulated high (above 5 cm) water depth a_h [m^2] (Equation S1 in Supporting Information S1) and the flooding area due to river water fraction presence (fractions above 0.1) a_{river} [m^2] (Equation S2 in Supporting Information S1). The values of a_h and a_{river} are calculated for each time step and used to calculate the correlation coefficient with the flooded area from the remote sensing data set. Further, we calculated the fraction of area that is indicated as flooded on the intersection remote sensing data set and water depths above 5 cm (i_h, Equation S3 in Supporting Information S1) and river water fractions above 0.1 (i_{river}, Equation S4 in Supporting Information S1).

2.7.3. Hydrochemical Validation

To investigate whether the different water sources presence is related to the simulated water source fractions we measured the electrical conductivity (EC) [μS cm^{-1}] of 133 samples in the floodplain during winter (24–25 January 2019) and spring (27–29 March 2019). The HI991300 portable EC meter was used and the location was recorded using a handheld GNSS receiver. We chose EC because prior research by Chormański et al. (2011) indicated that EC is effective at discriminating between river water and other sources. We used random 50% of

the measurement points to establish a linear regression model explaining the EC by the river, rain, snowmelt, and groundwater fractions in the model nodes on the measurement days. The remaining 50% of the data was used for validation of the linear regression model using RMSE [$\mu S\ cm^{-1}$] and bias [$\mu S\ cm^{-1}$]. All measurement points were used to calculate the correlation coefficients between the water source fractions and EC.

2.8. Changes of Water Sources Fraction in the Floodplain for the Past and Future Climate

Next to the simulated water sources fractions, we analyzed the mixing degree [-] (Berezowski et al., 2019), which quantifies the mixing between river and floodplain (sum of snow, rainfall, and groundwater) water fractions:

$$d = 1 - \frac{|f_{river} - f_{floodplain}|}{1 - f_{initial}} \qquad (4)$$

The changes in water sources fraction and mixing degree were assessed by calculating a length [days] of a period during which they were greater than 0.75 and the water depth was greater than 1 cm, in a hydrological year for each model node m in the floodplain:

$$l_s^m = \sum_{y=1}^{Y} \begin{cases} 1 & w_s^{y,m} > 0.75 \wedge h^{y,m} > 0.01 \\ 0 & \text{otherwise} \end{cases} \qquad (5)$$

where $w_s^{y,m}$ is a value of s water source fraction (river, snow, rainfall, or groundwater) or the mixing degree d during a day y of a all days Y in a hydrological year, and $h^{y,m}$ is water depth [m]. The total annual volume of surface water in the floodplain weighted by the water sources fractions and the mixing degree in a hydrological year was calculated by performing a weighted integration using the following equation:

$$v_s = \sum_{y=1}^{Y} \sum_{m=1}^{M} \begin{cases} h^{y,m} a^m w_s^{y,m} & h^{y,m} > 0.01 \\ 0 & \text{otherwise} \end{cases} \qquad (6)$$

The mean surface water depth $(\bar{h})$ [m] and the length of a period with water depth greater than 1 cm (l_h) [days] was calculated for each model node in each hydrological year. We chose the 1 cm depth threshold arbitrarily because the IHM simulates continuous (usually very low) surface water depth. This thresholding includes days in all periods with a depth greater than 1 cm, not only during the spring flood event, because inundation in different parts of the floodplain may occur multiple times or start and finish earlier or later than river flooding.

For future climate simulations, we calculated the above metrics for each EURO-CORDEX simulation and calculated the ensemble mean for each RCP scenario. Next, we used the ensemble means and historical simulations forced using 20CR data to calculate trends using the slope of the regression line, where the independent variable is the hydrological year. Finally, we used the t-test to investigate whether the trend estimate is significantly ($p < 0.05$) different from zero.

3. Results

3.1. Model Calibration

The hydrological model calibration results formed a clear Pareto front with a minimum RMSE of 0.19 m and maximum KGE of 0.86 (Figure S3 in Supporting Information S1). Out of these models we choose one with an RMSE of 0.24 m and a KGE of 0.69 as the best performing and used it for further simulations. The parameter search space was relatively wide for all material types, yet the saturated hydraulic conductivity presented an expected pattern with greater values for sands than for glacial till and relatively low value for peat (Table S8 in Supporting Information S1). As expected, the Manning roughness coefficient was calibrated to lower values in rivers with straighter course, located outside floodplain, than for Biebrza River.

3.2. Hydrological Validation

Simulated water levels and surface water discharge matched the observations well (Figure 3). Daily discharge at the Osowiec and Burzyn stations, which are located at the inlet and outlet of the floodplain were only slightly overestimated with an absolute error that was 5% of the data range (Table 1). Similar simulated discharge errors were also
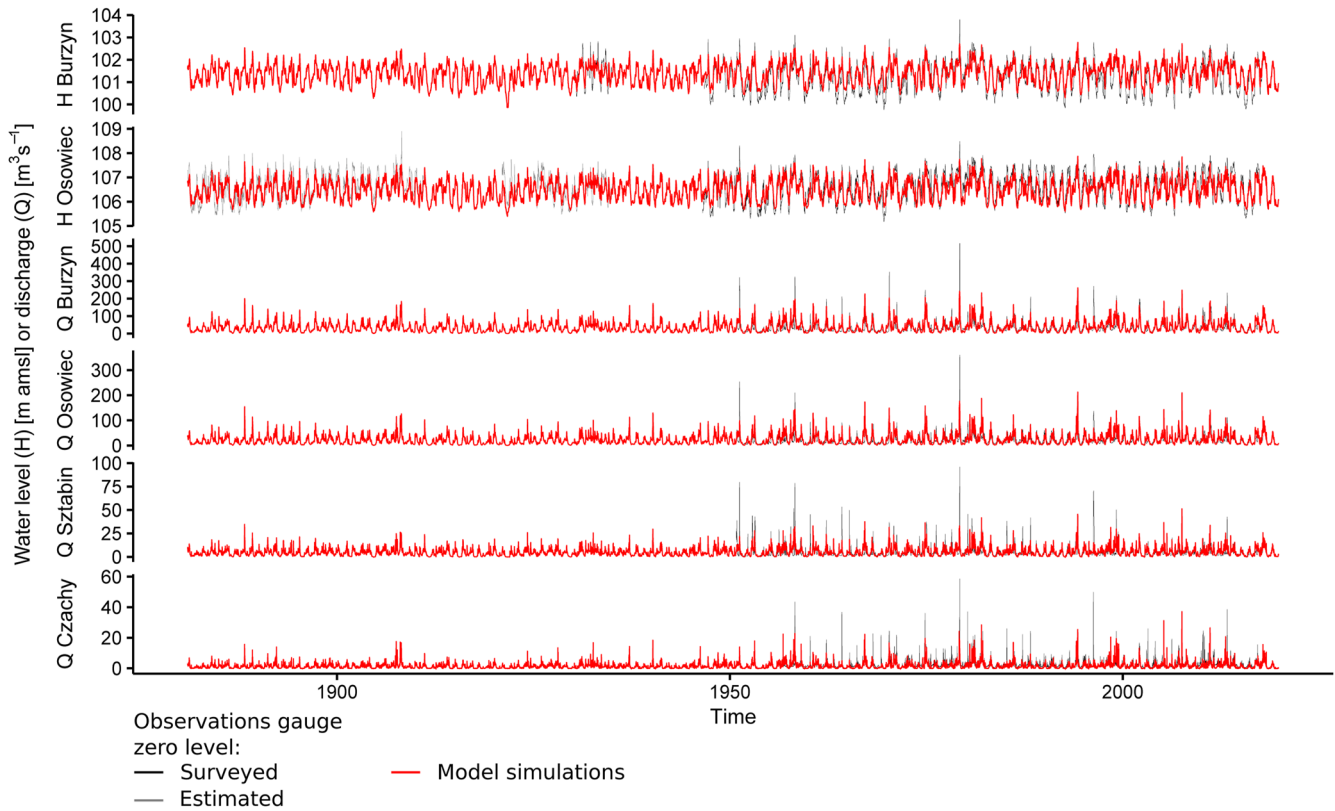
Figure 3. Simulated (red lines) and observed (black and gray lines) water levels (H) [m AMSL] and discharges (Q) [m³s⁻¹] for river gauges. The location of river gauges in presented in Figure 1 except for Sztabin, which is located in the upper part of Biebrza River. The yearly mean aggregation is presented in Figure S6 in Supporting Information S1.

present for Czachy, which is a major inlet into the floodplain, and Sztabin, which is located in the upper part of the catchment. Overall fit to observations expressed by KGE for discharge and water levels showed that Burzyn and Osowiec performed better than smaller stations Czachy and Sztabin. The high values of the correlation coefficient and the visual comparison shows that within-year and multi-year (Figure 3) variability of water levels was simulated correctly. The water levels RMSE were more attributed to high flows in Osowiec and low flows in Burzyn.

At the catchment scale, the model simulated groundwater levels very well, with the $r^2 = 0.99$ (Figure 4). Clear deviation of simulated groundwater levels was observed for the household wells located in the upland. Individual well's performance varied with the location in the model grid. In the floodplain, where the grid was finer than in the remaining parts of the model, the mean RMSE for nine wells was 23% of the data range with a 9%

Table 1
Error Metrics for all Available Observations for River Gauges

Station	Units	Period with observations	RMSE	RMSE/d.r.	Bias	Bias/d.r.	Corr.	KGE
H Burzyn	m	1930–1935, 1946–2017	0.37 (0.39)	9% (13%)	0.12 (0.09)	3% (3%)	0.84 (0.74)	0.69 (0.58)
H Osowiec	m	1881–1911, 1921–1923, 1925–1935, 1946–2017	0.36 (0.39)	11% (11%)	−0.17 (−0.11)	−7% (−3%)	0.83 (0.71)	0.70 (0.61)
Q Burzyn	m³ s⁻¹	1951–2017	25.88	5%	5.14	1%	0.69	0.64
Q Czachy	m³ s⁻¹	1957–2017	2.33	4%	−0.73	−1%	0.63	0.50
Q Osowiec	m³ s⁻¹	1951–2017	17.02	5%	2.79	1%	0.69	0.63
Q Sztabin	m³ s⁻¹	1951–2017	4.73	5%	0.84	1%	0.60	0.53

Note. Where applicable, the values were calculated separately for the period before (values in brackets) and after 1950. RMSE and bias are in the same units as indicated in the table, remaining metrics are dimensionless. H and Q are water levels and discharge respectively, RMSE/d.r. and bias/d.r. are RMSE and bias normalized to the observations data range (d.r.) in the analyzed period, corr. is the correlation coefficient.
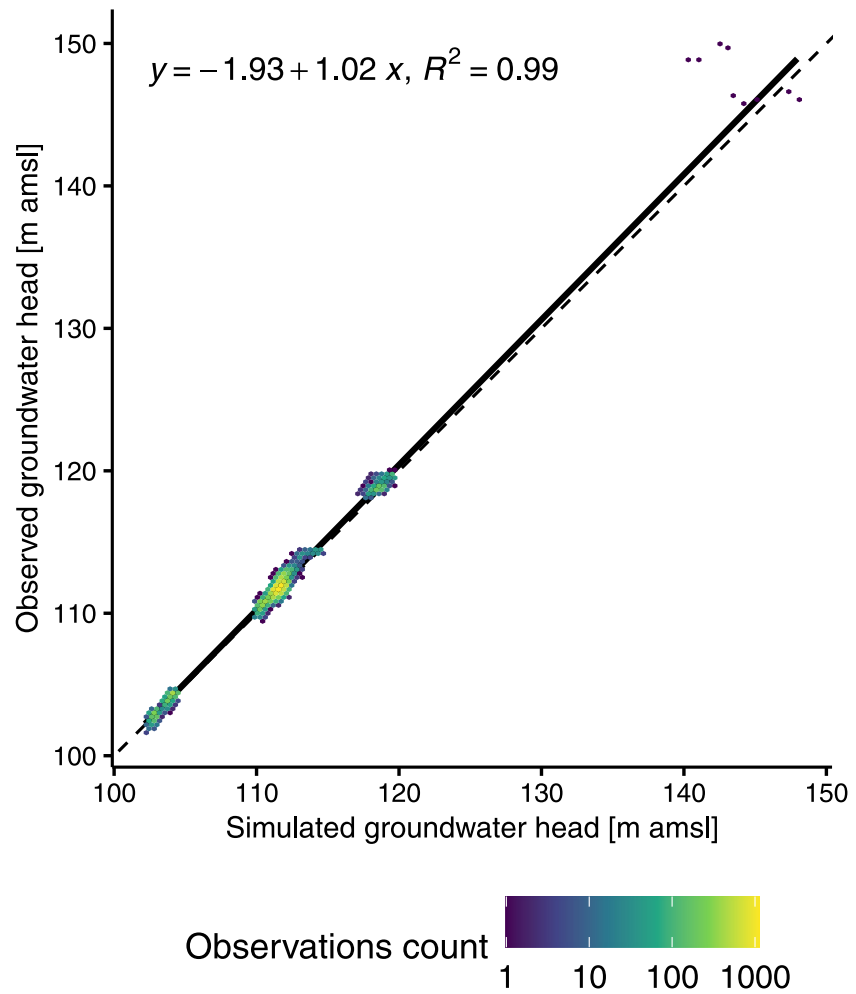
Figure 4. Validation of the simulated groundwater levels using daily observations (usually in 10 days resolution) in 43 wells in the period 1994–2019 ($N = 18{,}032$). Solid line - regression line, dashed line—1:1 line.

underestimation (Table S9 in Supporting Information S1). Outside the floodplain, that is, in the middle and upper parts of the Biebrza valley, the mean RMSE was 36% and 34% respectively (Table S10 in Supporting Information S1). In these parts of the catchment simulated groundwater levels performed worse for certain wells with RMSE up to 76% of the observed data range, although all wells preserved the temporal variability as in the observed data (Table S10 and Figures S7–S10 in Supporting Information S1).

3.3. Remote Sensing Validation

The temporal variability of the SAR water extent correlated better to the flooding extent derived from the river water fractions (a_{river}, $r = 0.75$) than to total extent estimated from the water depth (a_h, $r = 0.64$) (Figure 5a). Both a_{river} and a_h water extents overestimated the SAR flooding extent maps for the periods of the lowest water levels when the Biebrza River was not flooding. In these periods the remote sensing data -set was not indicating surface water extent (including between the river banks, Figure 6), while the total area of open water in Biebrza River and oxbow lakes in the floodplain is 2.97 km^2.

The higher correlation of SAR flooding extent maps with river water than with water depth was also visible spatially (Figure 5b). Along the river, the SAR data -set correlated stronger with the water depth than for the river water fractions. In the areas of dense vegetation, the correlation was low for both river water and water depth.

The Biebrza River and its tributaries were always visible in the hydrological model output what was not the case for the SAR data set (Figure 6). The hydrological model predicted a summer flood in 2017 that was not visible in
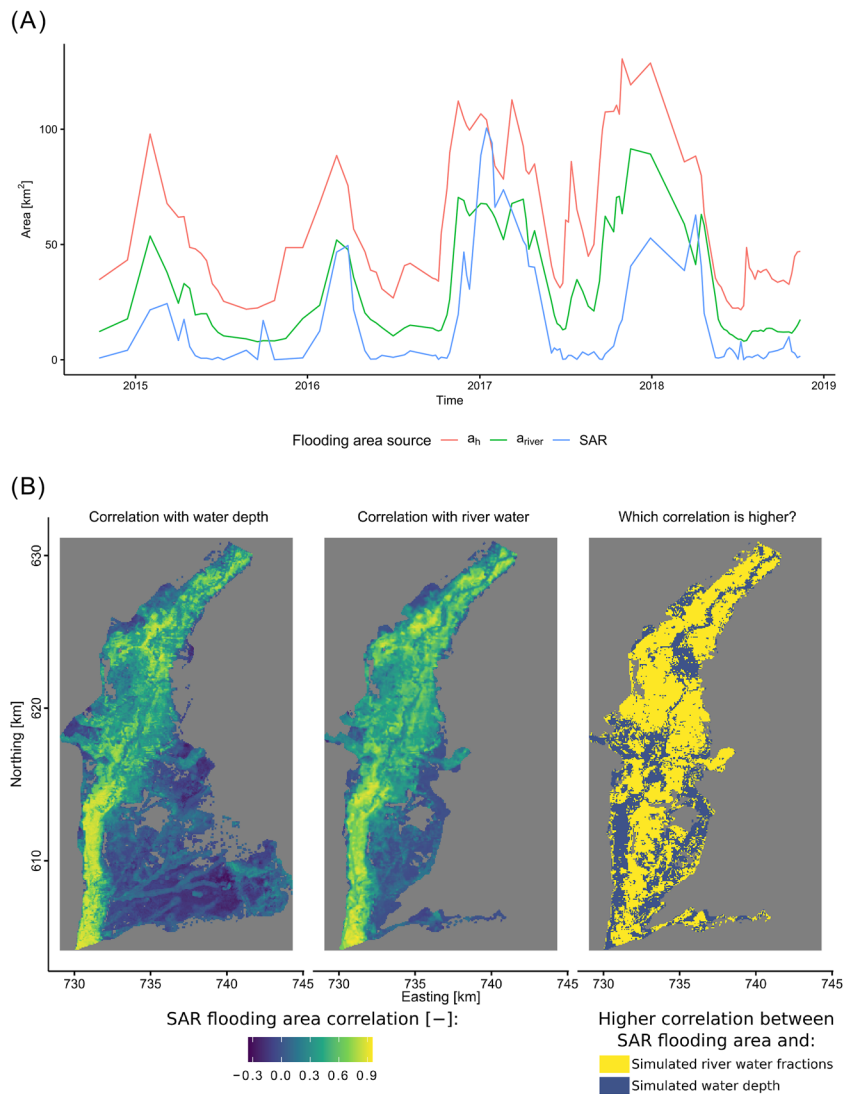
Figure 5. The total area of flooding extent from the remote sensing data set (synthetic aperture radar—SAR), was calculated for simulated water depths >5 cm (a_h) using Equation S1 in Supporting Information S1, and calculated for river water fractions >0.1 (a_{river}) using Equation S2 in Supporting Information S1 (a). Spatial correlation between time series SAR flooding extent maps and simulated water depth (left panel) and simulated river fractions (central panel) in the 2014–2019 period (b). The right panel shows in which places of the floodplain the correlation with river fractions was higher than with the water depth. The gray background indicates no valid correlation due to SAR flooding extent equal to zero (left panel), or river water fractions equal to zero over the entire period (central panel).

the SAR data (Figure 5). Also, one summer flood in 2015 visible in SAR data was not simulated by the hydrological model. There was a good agreement in the intersection of the true positive flooding extent from the remote sensing data set with simulated water depth $i_h = 0.77$ and with simulated river fractions $i_{river} = 0.78$. The lowest agreement occurred during low flow (below bankfull) periods with $i_h = 0.19$ and $i_{river} = 0.16$, while during higher flows (above bankfull) the agreement was higher $i_h = 0.82$ and $i_{river} = 0.83$.

3.4. Hydrochemical Validation

The correlation with EC measurements was strongly negative for snow fractions (−0.62) and moderately positive for the river fractions (0.48). A very weak correlation was observed for rainfall (−0.07) and groundwater (0.00). The linear regression model, which explained the EC measurements with the water source fraction predictors, showed that all fractions were significant (Table S11 in Supporting Information S1). The validation
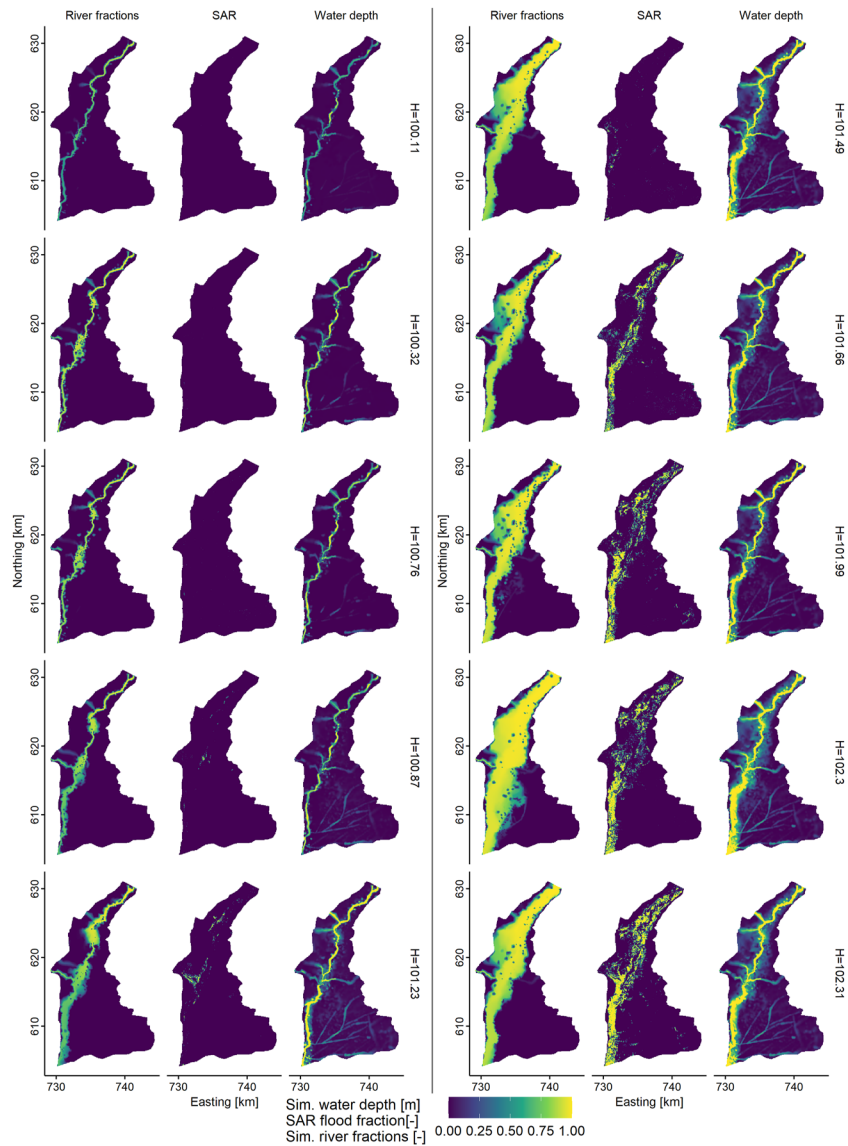
Figure 6. Flooding extent from remote sensing data set (synthetic aperture radar—SAR), simulated surface water depth, and hydraulic mixing-cell river water fractions for 11 increasing outlet water levels (H). Water depths >1 m were plotted as equal to 1 m in this plot to have consistency in the color scale.

metrics for the regression model (Figure 7) were $r^2 = 0.58$, RMSE = 91 µS cm^{-1} (18% of data range), and bias $b = 12$ µS cm^{-1} (2% of data range). The highest underestimation visible in the validation of the EC regression model was for measurements located next to an asphalt road located in a central part of the floodplain (~8.5 km from the Biebrza river, Figure 8).

3.5. Changes of Water Sources Fraction in the Floodplain for the Past and Future Climate

The simulated daily mean volume of water from different sources did not show significant trends for the past climate forced with the 20CR data (Figure 9). In the simulations forced by the EURO-CORDEX data for future climate positive trends were observed for the river, rainfall, groundwater, and river-floodplain mixed water volumes in RCP 2.6 and RCP 4.5. In the RCP 8.5 significant trends were observed only for rainfall and snowmelt volume. For all RCP snowmelt volume trends were negative, however, the trend was not significant for RCP 2.6. The snowmelt water was characterized by the lowest volume in the floodplain area and was subjected to the highest relative changes in the RCPs 4.5 and 8.5.
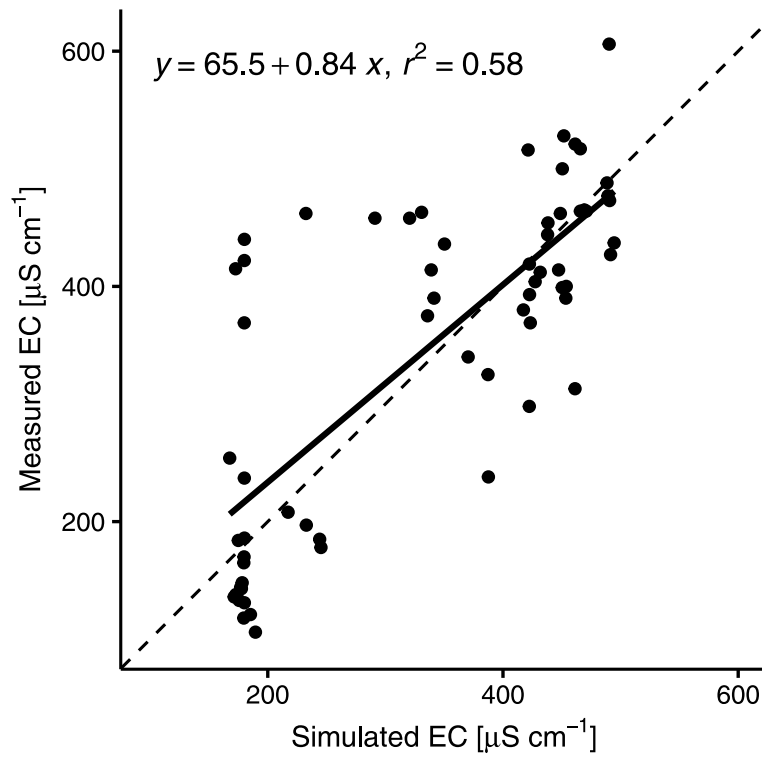
Figure 7. Validation of the electrical conductivity measurements regression model in the period 2019–2021 ($N = 64$). Solid line - regression line, dashed line—1:1 line.
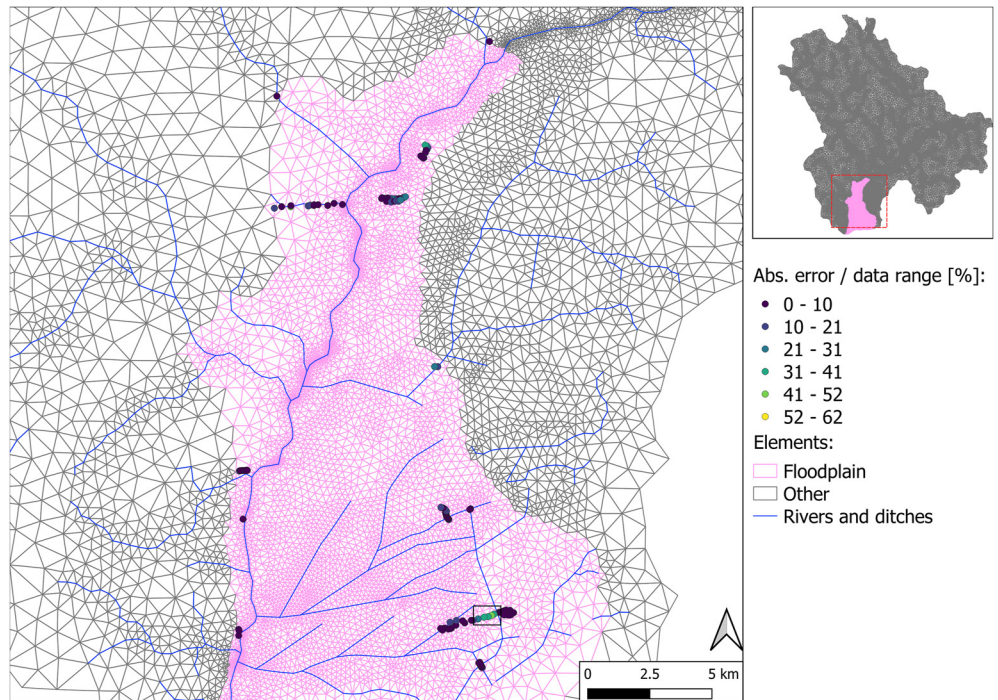

Figure 8. Errors of the electrical conductivity model for individual sampling points in the floodplain. The black square shows overestimated points in the proximity of an asphalt road. Both training and validation points are presented in this figure.
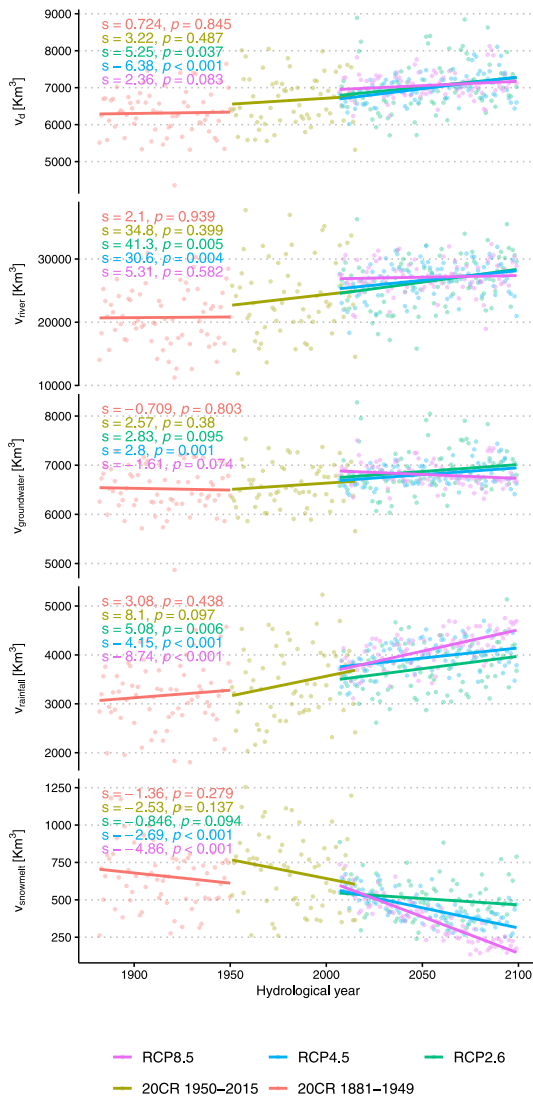
Figure 9. Simulated surface water volume daily means for river-floodplain mixing (v_d), river (v_{river}), groundwater ($v_{groundwater}$), rainfall ($v_{rainfall}$), and snowmelt ($v_{snowmelt}$) in the floodplain per hydrological year. The RCPs data is presented as the ensemble means. The s symbol is a slope of a regression line (trend) [Km³ year⁻¹] and the p symbol is a p value of a t-test for the slope estimate, 1 Km³ is 1,000 m³.

Length of a period in which water source fractions were dominant, the river-floodplain mixing degree was high, or water depth was greater than 1 cm was stable before 1950 with only a few nodes showing a slight increase for $l_{rainfall}$ (Figure 10). A similar situation was observed in the simulations for the 1950–2015 period. Therein, however, l_h and l_{river} increased in proximity to the Biebrza River. Also, $l_{rainfall}$ showed a more distinctive patch of increased values when compared to the latter period.

The trends for the ensemble mean in RCP 2.6 and 4.5 showed a similar pattern of increased l_h and l_{river} in the proximity of the Biebrza River and increased $l_{rainfall}$ in the central part of the floodplain (Figure 10). The increase of l_h and l_{river} was the greatest in RCP 2.6 out of all analyzed RCP scenarios and past climate periods. The increase of $l_{groundwater}$ was observed in RCP 2.6 near the valley margin, which was not visible for RCP 4.5. Unlike RCP 2.6, RCP 4.5 showed a decrease of $l_{groundwater}$ and $l_{snowmelt}$ in the central part of the floodplain.

The RCP 8.5 simulations showed that l_h and l_{river} was small and clearly smaller than in RCP 2.6 and 4.5 while the change of $l_{snowmelt}$ was similar as in RCP 4.5 (Figure 10. The decrease of $l_{groundwater}$ was the highest in RCP 8.5 and was visible in the central part of the floodplain (especially in the ditches), near the valley margin (northern part), and in the Biebrza River bed. Also, the increase of $l_{rainfall}$ was the highest in RCP 8.5 and was present in almost the entire floodplain.

In all simulations the length of the high river-floodplain mixing period, l_d, increased with increasing l_{river}, yet, the trend in l_d was smaller than the increase of l_{river}. An exception of this was in the central part of the floodplain in all RCP scenarios, where l_{river} did not show a significant trend, but l_d showed an increase. Therein $l_{rainfall}$ increased the most along with the $l_{groundwater}$ increase in RCP 4.5 and the $l_{groundwater}$ decrease in RCP 8.5. The l_d did not change nearest to the river in the RCP scenarios, whereas the l_{river} changed the most. In this area, l_d was high due to mixing at the beginning of the flood. The l_d also increased in the 1950–2015 period in the central part of the floodplain, west to the river.

The trend of surface water depth above 1 cm period, l_h, resembles that of l_{river} in the area where both trends were significant, that is, in the proximity of the river. The l_h, unlike l_{river}, increased also in the central part of the floodplain, especially in the ditches, and next to the valley margin in all RCP scenarios and a few nodes in the 1950–2015 period. The highest l_h increase in these areas was observed in the RCP 2.6, although the change in $l_{snowmelt}$, $l_{groundwater}$, and especially in $l_{rainfall}$ was the smallest in this scenario among all RCPs. Overall, the magnitude of l_h change was the highest in RCP 2.6 (accompanied by the highest magnitude of l_{river} change) although the area of significant changes was greater in remaining RCPs. Notably, in the areas where l_d increased, but l_{river} trend was not significant the l_h also showed an increase. Still, l_h increased in areas further away from the river where neither l_d nor l_{river} increased.

Significant trends in mean daily water depth, $\bar{h}$, were observed spatially only in the RCP scenarios for the future climate (Figure 11). The trends were the greatest in the proximity of the river, reaching some river nodes up to 6.3 mm year⁻¹ in RCP 2.6, 4.0 mm year⁻¹ in RCP 4.5, and 0.7 mm year⁻¹ in RCP 8.5 (Figure 11). The RCP 4.5 and 8.5 scenarios predict a very small positive trend across the majority if the floodplain, whereas RCP 2.6 predicts such a trend only in remote parts of the floodplain and in ditches.
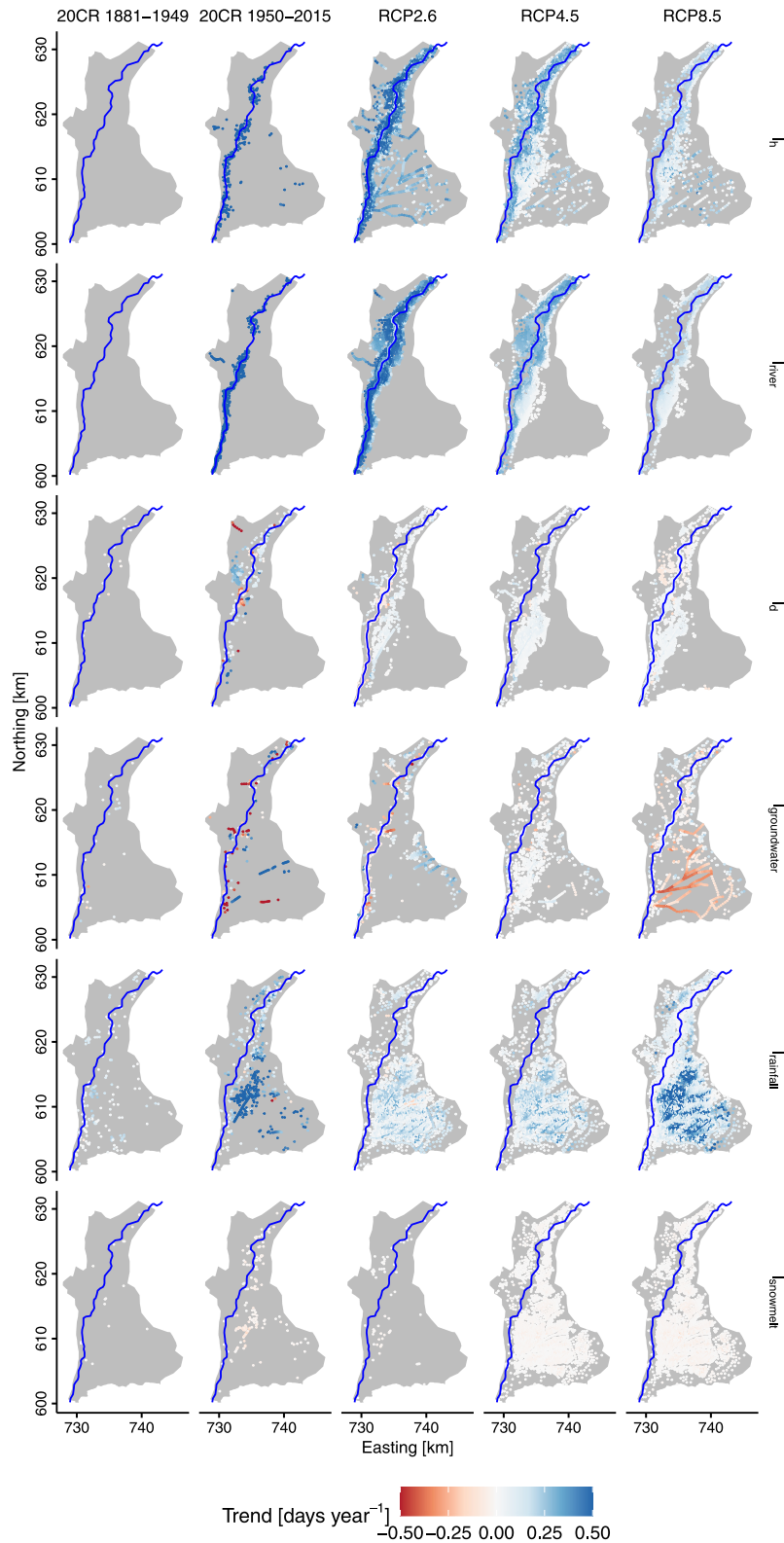
Figure 10. Changes of the period's length when water depth, h, is greater than 1 cm (l_h), river water (l_{river}) or floodplain water ($l_{groundwater}$, $l_{rainfall}$, and $l_{snowmelt}$) fractions are greater than 0.75, and the river-floodplain mixing degree, d, is greater than 0.75 (l_d) annually. Only model nodes with significant trends ($p < 0.05$) are shown. The gray polygon is the floodplain area, the blue line is the Biebrza River; tributaries and ditches are not shown for clarity, please refer to Figure 1 to identify their course.
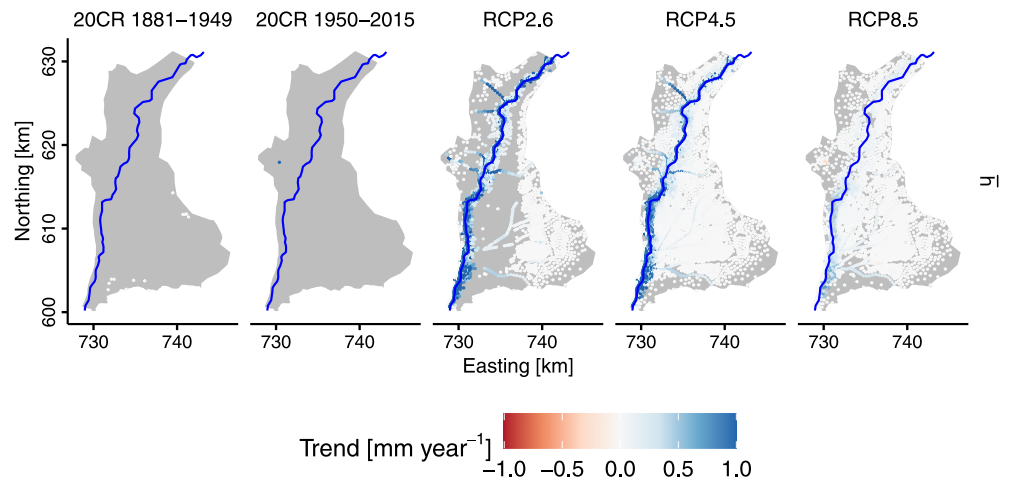
Figure 11. Changes in the annual mean daily water depth, $\bar{h}$. Only model nodes with significant trends ($p < 0.05$) are shown. The color scale is clipped to the $<-1, 1>$ mm year^{-1} range, and the values outside this range are colored as equal to -1, or 1 mm year^{-1}; the clipping affected 15% of the data in representative concentration pathways (RCP) 4.5% and 30% of the data in RCP 2.6 located in the proximity of the river. The Gray polygon is the floodplain area, the blue line is the Biebrza River; tributaries and ditches are not shown for clarity, please refer to Figure 1 to identify their course.

4. Discussion

4.1. Model Validation and Performance

The multi-site validation presented in this study showed overall good performance of dynamic hydrological processes simulated in the model. However, a model performance degradation, such as increased RMSE for groundwater heads and decreased KGE for discharge, was observed outside the floodplain area (in the middle basin, upper basin, and upland). This was primarily a result of using a finer grid in the floodplain and a coarser grid elsewhere. A fraction of the error may be attributed to errors in the elevation of the groundwater wells or the DEM used for the model. More discussion on the model development and calibration is presented in Section S3.1 in Supporting Information S1.

From the flooding perspective, the model satisfactorily predicted the above bankfull flow conditions and the majority of high flow events. However, the model was unable to correctly simulate five large flood events (or 7.6% of floods in the 1951–2017 period) with the highest discharge peaks (above 250 m^3 s^{-1}). We hypothesize that the inability to simulate the highest peak discharges is primarily due to the coarse resolution ($1° \times 1°$) of the 20CR forcing data and limitations of bias correction. Notably, 30% of RMSE reported for the Burzyn station water levels was attributed to the bias that occurred during low flow conditions and was not relevant for the flooding analysis. If only the above bankfull conditions were taken into the error calculation the RMSE would decrease to 0.26 m, that is, 6.5% of the observed water levels. Therefore, our model has demonstrated the capacity to predict normal hydrological behavior including flood events with return periods below 13 years.

The model performance before 1950 was evaluated based on water levels in Burzyn and Osowiec stations, where the absolute water levels were estimated from the relative records. Because of that only the correlation coefficient, which does not account for the absolute values, is a model performance quantifier that can be used for comparison between the pre-1950 and post-1950 periods. Nonetheless, the correlation was lower in the pre-1950 period than in the post-1950 period. This could be due to higher errors related to a lower number of atmospheric pressure observations in the 20CR forcing data set (Slivinski et al., 2019). Another explanation could be that the morphology of the river changed between 2012 (the year of the river cross-section measurements) and the 1881–1949 period. We had no reliable data source for historical or for future periods hence we were not able to include the river morphology change in the model. Still, the model is suitable for analysis of long historical and future periods for the floodplain inundation composition. This is because the floodplain area has not changed considerably since 1881 and is expected not to change in the future due to historical and future-projected low human impact, conservation practices, and the fact that all melioration works were carried out before 1881.

To summarize, the validation of the model for the pre-1950 and post-1950 periods in the floodplain did not show a considerable decrease in performance. Therefore, the fact that we used a very short calibration period in

reference to validation, and simulation periods shows the skill of the model to predict hydrological conditions for the periods (past or future) with some morphological changes in the river. If we would increase the calibration period, the errors in the pre-1950 period could possibly be lower because the parameters would account for the morphological changes. This would, however, result in a less physical meaning of the parameters, the simulation errors not being quantitative for the future RCP periods, and a less representative simulation of the future RCP periods (due fit of the model to historical morphology).

The SAR flooding area correlated more strongly with the river water than with the total (due to water depth) flooding extent. Spatially, the correlation between the SAR data set and river water was generally higher than with the water depth. An exception to this was the belt around the river, where the water depths varied the most and river fractions were always close to one. The reason for this was that the SAR data set was unable to detect water below vegetation, that is in the areas where water depths were noticeable, but low. Since river water fractions are also lower in these areas than in the river proximity they are in agreement with the SAR data set which indicated no flooding. This shows that the SAR data set in the densely vegetated Biebrza floodplain shows mostly the river water extent rather than the total inundation. Hence the SAR data set can be used to track mostly the extent of river water flooding. Nonetheless, good temporal correlations of the total flooding area, and flooding area due to river water with the SAR data set flooding area, show that the flood dynamics simulated with the IHM and HMC agree with the observed phenomenon.

The EC of water was another, next to the SAR data set, spatial and temporal validation data source. Unlike the remaining validations, the EC was used as an indicator of the water source. The model based on the HMC water source fractions predicted EC spatially with low errors except for the area located in the proximity of an asphalt road. The errors were present in the direction of water flow from the road, which offers an explanation to the reason for the errors as likely being the pollution due to car traffic. Our results show that EC correlated positively with river water fractions and negatively with snowmelt water fractions. This is because EC has higher values in the river than in floodplain water (Chormański et al., 2011). Further, the hydrochemical validation shows that all water source fractions are significant predictors of surface water EC and that the RMSE for EC validation was low, which indicates that the simulated fractions agree spatially and temporarily with the true water source. This is in line with our previous study (Berezowski et al., 2019) conducted for a single flooding event on a coarser grid showed that the simulated fractions agree with water sources derived from a multi-parameter hydrochemical analysis.

Our model passed the comprehensive (Gelfan et al., 2020; Krysanova et al., 2018), multi-source and long-term validation. Such validation was required because the simulation of water mixing, which is a product of interaction between climate, groundwater, and river flooding, requires more confidence in the modeling results than just agreement with observed water levels or discharge.

A limitation of the future climate simulation performed in this study is that we used fewer EURO-CORDEX models in the RCP 2.6 ensemble than in RCP 4.5 and 8.5 ensembles. The IHM and HMC water mixing results were calculated as the ensemble mean from simulations forced by each EURO-CORDEX model in each RCP. Therefore, in the five-model ensemble for RCP 2.6, the influence of individual EURO-CORDEX model on the results is greater than in 10 model ensembles in RCP 4.5 and 8.5. Effectively the uncertainty of the results of this study in the RCP 2.6 is greater than in RCP 4.5 and 8.5. Due to a lack of data, we were not able to use more models in RCP 2.6, however, we tested the sensitivity of the results to a decreased number of models in ensembles for RCP 4.5 and 8.5. Our analysis showed that when the same five models were used in RCP 4.5 and 8.5 as in RCP 2.6 the trends in water sources fractions and water levels in the floodplain (Figures S11 and S12 in Supporting Information S1) are very alike as in the original 10 model ensembles (Figures 10 and 11). The difference, however, was in the number of significant trend locations, which was greater in the ten-model ensemble. This means that in both cases the same pattern of trends in visible in the results, while the ten-model ensemble shows the same direction of change in the IHM results over a greater floodplain area than the five-model ensemble.

4.2. Changes of Water Sources Fraction in the Floodplain for the Past and Future Climate

Water source fractions were stable in the 1881–2015 period in terms of the lumped volumes of water. This situation was expected, because the 20CR forcing data also did not had any trends in this period. On the other hand, the spatial trends in the water sources fractions persistence showed trend for some spots for rainfall in the 1881–1949 period and, more interestingly, for all fractions and water depth in the second part of the 20th century. These trends (except for groundwater) coincided with the spots where the trends were present in future periods RCPs.

In the RCP 2.6 lumped volume of river and rainfall water significantly increased during the 2005–2099 period. An increase in rainfall with a significant, but eightfold smaller decrease in snowfall, and no change in PET resulted in overall wetter conditions. This translated not only to increased river discharge, and high river fraction persistence but also to longer-lasting high groundwater fractions and surface water depth. Effectively, the period of river-floodplain water mixing was longer in the proximity of the river by forming a clear belt and resulting in a significantly increased volume of mixing water.

A similar situation was observed in RCP 4.5, but due to a twofold higher decrease of snowfall and similar magnitude of rainfall trend as in RCP 2.6 period of high snowmelt fractions shortened during the 2005–2099 period. In addition to that, a greater decrease in PET in RCP 4.5 than in RCP 2.6 resulted in less wet conditions. As a result, a lesser trend of river discharge and water levels was observed. Since groundwater discharge is more related to overall drier or wetter conditions rather than to instantaneous fluxes of water the decrease in snowmelt water resulted in longer dominance of groundwater fractions in the river proximity in RCP 4.5. Despite drier conditions in RCP 4.5, the longer periods of groundwater, rainfall, and river fractions in this area affected in the river-floodplain mixing zone last longer in greater areas than in RCP 2.6.

A different situation was observed in RCP 8.5, where snowfall nearly ceased and the increase of rainfall was in great part balanced by the increase of PET resulting in no trends observed in discharge or water levels in the 2005–2099 period. The stability of discharges was not accompanied by the stability of the lumped volume of water from different sources, as rainfall volume increased and snowmelt volume decreased. Spatially, the most distinctive pattern of high groundwater fractions persistence decrease was observed in RCP 8.5. Such a big groundwater fraction decrease is an indicator of drought conditions locally in the central part of the floodplain. This was however balanced by longer persistence in the northern part of the floodplain and near the valley margin, resulting in no significant trend in the lumped volume of groundwater.

The spatial trends in mean water depth and inundation period length did not align with the trends of water source fractions. Overall, the trends of mean water depth were rather small except in the river proximity. Also the spatial trends of water source fractions also did not aligned with the trends of water levels and discharge at the catchment outlet, which, if significant were all positive for the past and future climate forcing data (Text S5 in Supporting Information S1). This shows that the variability of floodplain water composition and water depth is governed spatially not by river flooding directly, but by local precipitation, snowmelt, and groundwater discharge patterns.

The trends in the forcing data, lumped volumes, and spatial persistence of water source fractions often showed not aligned direction, or were not significant when not analyzed spatially. This indicates that processes leading to a dominant presence of water source in the inundation cannot be directly concluded from the forcing data. Moreover, the lumped analysis of water volumes, which would be available from simpler hydrological models than the IHM used in this study, fails to depict spatial contrast in trends, and due to averaging often shows no climate change impact. An exception to this was the snowmelt water which only showed significant decreasing spatial trends, which was in line with decreasing snowfall and decreasing lumped snowmelt volume in RCPs 4.5 and 8.5 and with the forcing data. To summarize, a physical model, which simulates interactions in the water cycle spatially and integrates different climatic forcing, like the IHM used here, is required to fully understand the impact of climate change on the complex process of water mixing in the floodplain.

4.3. Implications for Modeling

As illustrated in our study, the period of inundation with water depth above 1 cm, was also influenced by climate outside the river water flooding zone. Moreover, the trend of this period was not correlated to the distance from the river, as it increased near the river, then decreased, and increased again in the central part of the floodplain (RCP 4.5 and 8.5), or it increased in the entire floodplain (RCP 2.6). The trend in water depth change was correlated to the distance from the river, however, significant positive trends were observed both in areas dominated by the river and floodplain water. Furthermore, water depth trends in RCP 2.6 showed that large areas of the floodplain did not have any trends, while the most remote parts of the floodplain had a significant positive trend. This depicts important advantage of IHMs, which is the representation of water depths in the entire floodplain. Hydrodynamic models for 2D surface water routing perform very well in simulating river water flooding extent, whereas, are unable to simulate inundation from other sources, such as groundwater, without coupling with different models (Appledorn et al., 2019). Still, some studies use a surface-water-only model to analyze long-term

floodplain inundation changes (Veijalainen et al., 2010; Wen et al., 2013). While in some areas a lack of groundwater coupling may not influence the results, in other areas it may be a source of bias in simulated inundation extent.

4.4. Implications for Ecological Processes

Mixing of water from different sources creates biogeochemical hot spots and hot moments, such as denitrification (McClain et al., 2003). Several studies have analyzed denitrification spatially in inundated floodplains to reveal that it is strongly affected by connectivity with river water (Forshay & Stanley, 2005; Jones et al., 2014; Racchetti et al., 2011; Scott et al., 2014). The connectivity enables shift from oxic conditions in a nitrate-rich river water to hypoxic conditions in the floodplain water. In such conditions denitrification bacteria reduce nitrate to molecular nitrogen. Our study shows that the river-floodplain water mixing volume, extent, and persistence varies with climate change, therefore denitrification patterns in Biebrza and similar floodplains can also be affected. For example, a shift in precipitation patterns for the Atchafalaya River (Jones et al., 2014) could lead to decreased groundwater discharge and rainfall pounding in the backwater wetlands, which would effectively decrease the denitrification of river water. This variability was visible much better in the spatial pattern than in the lumped, water volumes. Therefore, improvement in denitrification modeling at floodplain (Hallberg et al., 2022) or catchment (Adame et al., 2019) scale or in the use of scaling relationships (O'Connor et al., 2006; Tomasek et al., 2017) could be achieved by introducing additional variables related to groundwater discharge, precipitation water, or the river-floodplain mixing extents.

In the Biebrza floodplain the river-floodplain water mixing volume increased the most in the RCP 2.6 and 4.5. Spatial analysis showed that in each RCP scenario high mixing degree will persist longer in a broad belt around the Biebrza River, which corresponds to the intersection of longer persistence of river fractions and floodplain water sources. Bacteria from Gammaproteobacteria taxonomic group, of which some species are known to perform denitrification (Baker et al., 2015) were found in oxbow lakes in the floodplain (Lew et al., 2016). Therefore, the mixing of river water subsequently with the oxbow lakes and inundation in the Biebrza floodplain may promote conditions suitable for denitrification over larger area and in greater volume in the future climate RCP 2.6 and 4.5 than currently and in the past. A study on denitrification bacteria for the Garonne River wetlands shows that their pattern is dependent on flooding and water chemistry (Iribar et al., 2015). Hence, alteration of water source extents during floods may also lead to a change of denitrification bacteria composition in other study areas than Biebrza.

Another process, that is related to the extent of water from different sources is vegetation development (Keizer et al., 2014; Park & Latrubesse, 2015). Modeling of vegetation development under climate change may be hampered because studies using the process-based model (Politti et al., 2014), a statistical approach (Mosner et al., 2015) do not include hydrodynamic feedback between water from different sources while focusing only on the river, or groundwater levels. As shown by Gattringer et al. (2019) predictors from an IHM improve habitat modeling in comparison to groundwater, or surface-water-only predictors scenarios. Our results indicated that in some scenarios the trends were not present in water levels, or discharges while they were present in the persistence of dominant water sources. Therefore, we believe, that the inclusion of water source extents predictors could improve vegetation models further. We are not aware of any study that used IHM-simulated water sources to model vegetation development or distribution.

Interactions between water sources influence the surface water velocity field in the floodplain in reference to a situation when river water is the sole inundation source. The velocity field affects the sedimentation pattern in the floodplain due to the settling velocity parameter of the suspended particles. The lower the settling velocity the more time is required for sedimentation on the floodplain. Therefore, the mixing degree, which shows where river and floodplain water with different momentum mix, and the river water extent, which shows the overall area of sedimentation from river water, can indicate hot spots of sedimentation. A recent study conducted in the Biebrza floodplain revealed that the vegetation productivity was associated with the zone of nutrient rich sediment deposition (which is a part of the river water zone located close to the river) rather than by the total inundation extent (Keizer et al., 2018). Thus the mixing zone and the river water zone are candidates for high-productivity vegetation zone predictors in temperate floodplains and can possibly be used to model climate impact on floodplain vegetation.

Our results show that the period of high river-floodplain water mixing increased the persistence in the central part of the floodplain in the 1950–2015 period. Notably a vegetation shift was observed in that area from high

sedges in 1980 to Caricion demissae in 2000 (Berezowski et al., 2018). However, in other areas where this vegetation shift was observed, we did not observe trends in the period of high river-floodplain water mixing. We also observed a clear pattern of increased persistence of river water around Biebrza River which corresponds spatially to the vegetation shift from high sedges in 1980 to reeds in 2000 (Berezowski et al., 2018). Reeds have higher biomass than high sedges and this parameter was positively correlated with the nutrient deposition from river sediments in the Biebrza floodplain (Keizer et al., 2018). Our results also show that the groundwater zone will decrease in RCP 8.5. This can result in the loss of the sedge-moss vegetation, which is related to the groundwater dilution zone in the floodplain (van Loon et al., 2009). Notably, during the above mentioned historical periods, the water level trend was not present in the floodplain. This shows that the spatial identification of water sources we performed in this study can be linked to ecological processes that occur in the floodplain. This also shows that vegetation modeling can be an application of the water source fractions simulated by HMC, while water levels, which are often used to model vegetation distribution, do not show spatial or temporal change. Yet, to identify the relationships between the water source fractions and vegetation a spatial model would be required, which was not in the scope of this study.

The floodplain features many paleochannels and oxbow lakes with various levels of connectivity to the main river. In Biebrza River the water chemistry in the oxbow lakes is related to bacteria, zooplankton, and fish population and can be an effect of contact with different water sources (Glińska-Lewczuk et al., 2016; Grabowska et al., 2014; Lew et al., 2016). The ecological functioning of oxbow lakes was not assessed directly in the scope of water sources except for speculations that snowmelt water can dilute nutrients in the oxbow lakes and affect the bacteria division rate Lew et al. (2016). Our results suggest that the effect of different water sources present in the inundation can be broader than dilution, as in general, groundwater not only dilutes river water but also is characterized by lower oxygen concentration and higher concentration of minerals than in the river water. In this scope, the oxbow lakes in the floodplain will be the most affected by the elongated persistence of high river water fractions in RCP 2.6 and 4.5 in the area along the river. Based on the former research longer periods of increased nutrients and oxygen concentration could directly lead to an increase in bacteria richness (Lew et al., 2016), alteration of zooplankton species (Grabowska et al., 2014), and increase in fish abundance (Glińska-Lewczuk et al., 2016).

Climate change in Europe during Holocene resulted in increased stream power and sediment load, which affected in creation of meanders or the transition between meandering and anastomosing rivers (Słowik, 2022). In case of the analyzed floodplain the current meanders and paleochannels in the fluvial terrace are relatively new and were developed along with increasing peat deposition during younger Holocene which now covers the effects of river activity during older Holocene and Pleistocene (Banaszuk & Micun, 2009). Climate-driven changes in river discharge can have a substantial impact on channel morphology and consequently on floodplain inundation and sedimentation (Slater et al., 2019; Slater & Singer, 2013). Yet, there is not much evidence on how the variability of remaining water sources due to climate change could directly affect the geomorphological features of floodplains except for different forms of erosion (Aalto et al., 2003; Shellberg et al., 2013). To assess the effect of water sources on the floodplain morphology a hydromorphological model would be required, what was outside the scope of this study.

4.5. Implications for Management

The Biebrza floodplain, as part of a national park, has been subjected to active protection measures. An increase in water levels through the construction of dams, or vegetation removal by mowing, allowed, to some extent, to diminish the potential effect of climate change in this area (Berezowski et al., 2018). Our results together with other experiments discussed herein show that the analysis of water sources and their mixing may have a considerable ecological effect. However, at this point, more models are needed to asses this effect more precisely spatially and temporarily. Therefore, the current local management strategy could be to increase the resilience of the wetland ecosystem and implementation of adaptive management (Lawler, 2009). Except that, the local management strategies may be somewhat challenging, as tools for preserving the shape and duration of water sources' zones are limited. On the other hand, our results have shown that the spatially distributed trends in water source fractions were driven solely by climate change, as our model neglected other divers (water use, land-use change, etc.). Therefore, global actions limiting climate change impact on wetlands driven by national and international policies (Moomaw et al., 2018) seem to be an appropriate measure to limit the shift in the extent of water from different sources.

4.6. Note on Hardware Requirements

The simulations were run on the Tryton cluster, which has 3,215 Intel Xeon Processors (E5 v3, 2.3 GHz, 12-core) with 128 GB RAM, resulting in a total of 1.792 PFLOPS. We split the simulations into 978 smaller tasks (a three-year simulation period with a 2-year warm-up period), to use the resources in parallel and to fit into 72 hr wall time for a single simulation. The cluster resources were shared with other users therefore it took about 5 months to finish all computations. The total output data produced by the models accounted for about 20 TB.

5. Summary and Conclusions

Simulations of surface water source fractions in a natural wetland floodplain over a two-century period reveal that by 2099 the projected future climate change will significantly alter the patterns that were relatively stable in the 1881–2015 period. Our results show that analysis of the lumped output of the model was less sensitive to depict the climate change effect that was visible when the trends were analyzed spatially in the floodplain. Different future climate scenarios showed very variable impacts on water source fractions, which were often counterintuitive. In the RCP 2.6, which projected the least climate change in the study area, we observed the highest magnitude of changes related to the increase in river discharges, water levels, and river water fractions. In the RCP 8.5 scenario, which projected the greatest increase in PET and rainfall accompanied by the greatest decrease in snowfall, these trends were less significant, while only this scenario projected dry conditions exhibited by a decrease of groundwater fractions in the inundation. The trends in water source fractions had different spatial patterns and showed greater sensitivity to climate change than trends in water depth and inundation duration.

This complex hydrological impact was simulated by the IHM, which allowed us to model interactions between groundwater and surface water and limit the assumptions about hydrological fluxes in the top layer of the model to the meteorological forcing. This is the first study that simulated the climate impact on water source fractions in the inundation and the longest application of IHM in terms of the simulation period. Hydrological impact studies are always related to uncertainty, which we limited here by multi-variable verification and projection of future impact using an ensemble of 10 EURO-CORDEX simulations (only 5 in RCP 2.6).

We showed that the water source fractions are sensitive to the climate in a natural temperate zone wetland floodplain. This fact has several implications for other modeling studies, ecological processes, and management in similar wetlands. Modeling problems should be carried out using IHMs to depict proper inundation or sedimentation patterns spatially, because, even if the water sources fractions are not explicitly simulated using HMC, IHMs capture the interactions between water from different sources which produce inundation outside the river water zone and changes the velocity field. Since ecological processes, such as denitrification, microorganisms and fish abundance, or vegetation development, are in part related to water sources' zonation and their mixing, these variables should be taken into account in models, especially in climate change impact studies. Finally, the managers have limited tools in shaping the surface water zonation and extent, therefore except for increasing the wetlands resilience, and adaptive management using an IHM output, global actions aimed at decreasing climate change impact should be the main priority.

Authority of Poland (Wody Polskie) through a web portal (Polish Goverment, 2019). The EURO-CORDEX future climate data is available in (EURO-CORDEX, 2019). PET data was provided by the Joint Research Center and is available in (Joint Research Center, 2019). CORINE Land Cover map was provided by the European Commission and is available in (Commission of the European Communities, 2013).

References

Aalto, R., Maurice-Bourgoin, L., Dunne, T., Montgomery, D. R., Nittrouer, C. A., & Guyot, J.-L. (2003). Episodic sediment accumulation on Amazonian flood plains influenced by El Nino/Southern Oscillation. *Nature*, *425*(6957), 493–497. https://doi.org/10.1038/nature02002

Adame, M. F., Roberts, M. E., Hamilton, D. P., Ndehedehe, C. E., Reis, V., Lu, J., et al. (2019). Tropical coastal wetlands ameliorate nitrogen export during floods. *Frontiers in Marine Science*, *6*. https://doi.org/10.3389/fmars.2019.00671

Anonymous. (2019). Public data, period: 1951-2019 [Dataset]. https://danepubliczne.imgw.pl/data/dane_pomiarowo_obserwacyjne/

Appledorn, M. V., Baker, M. E., & Miller, A. J. (2019). River-valley morphology, basin size, and flow-event magnitude interact to produce wide variation in flooding dynamics. *Ecosphere*, *10*(1). https://doi.org/10.1002/ecs2.2546

Arnell, N. W., & Gosling, S. N. (2016). The impacts of climate change on river flood risk at the global scale. *Climatic Change*, *134*(3), 387–401. https://doi.org/10.1007/s10584-014-1084-5

Baker, B. J., Lazar, C. S., Teske, A. P., & Dick, G. J. (2015). Genomic resolution of linkages in carbon, nitrogen, and sulfur cycling among widespread estuary sediment bacteria. *Microbiome*, *3*(1), 14. https://doi.org/10.1186/s40168-015-0077-6

Banaszuk, H. (2004). Kotlina biebrzanska i biebrzanski park narodowy. *Bialystok Ekonomia i Srodowisko*. (In Polsih).

Banaszuk, H., & Micun, K. (2009). Formation and evolution of river valleys in large melt-out depressions in the North Podlasie lowland. *Prace i Studia Geograficzne*, *41*, 25–36. (In Polish).

Barthel, R., & Banzhaf, S. (2015). Groundwater and surface water interaction at the regional-scale—A review with focus on regional integrated models. *Water Resources Management*, *30*(1), 1–32. https://doi.org/10.1007/s11269-015-1163-z

Berezowski, T., Bieliński, T., & Osowicki, J. (2020). Flooding extent mapping for synthetic aperture radar time series using river gauge observations. *IEEE Journal of Selected Topics in Applied Earth Observations and Remote Sensing*, *13*, 2626–2638. https://doi.org/10.1109/JSTARS.2020.2995888

Berezowski, T., Partington, D., Chormański, J., & Batelaan, O. (2019). Spatiotemporal dynamics of the active perirheic zone in a natural wetland floodplain. *Water Resources Research*, *55*(11), 9544–9562. https://doi.org/10.1029/2019wr024777

Berezowski, T., Wassen, M., Szatyłowicz, J., Chormański, J., Ignar, S., Batelaan, O., & Okruszko, T. (2018). Wetlands in flux: Looking for the drivers in a central European case. *Wetlands Ecology and Management*, *26*(5), 849–863. https://doi.org/10.1007/s11273-018-9613-z

Boko, B. A., Konaté, M., Yalo, N., Berg, S. J., Erler, A. R., Bazié, P., et al. (2020). High-resolution, integrated hydrological modeling of climate change impacts on a semi-arid urban watershed in Niamey, Niger. *Water*, *12*(2), 364. https://doi.org/10.3390/w12020364

Brunner, P., & Simmons, C. T. (2012). Hydrogeosphere: A fully integrated, physically based hydrological model. *Ground Water*, *50*(2), 170–176. https://doi.org/10.1111/j.1745-6584.2011.00882.x

Chormański, J., Okruszko, T., Ignar, S., Batelaan, O., Rebel, K., & Wassen, M. (2011). Flood mapping with remote sensing and hydrochemistry: A new method to distinguish the origin of flood water during floods. *Ecological Engineering*, *37*(9), 1334–1349. https://doi.org/10.1016/j.ecoleng.2011.03.016

Commission of the European Communities. (2013). Corine land-cover [Dataset]. http://www.eea.europa.eu/publications/COR0-landcover

Erler, A. R., Frey, S. K., Khader, O., d'Orgeville, M., Park, Y.-J., Hwang, H.-T., et al. (2019). Evaluating climate change impacts on soil moisture and groundwater resources within a lake-affected region. *Water Resources Research*, *55*(10), 8142–8163. https://doi.org/10.1029/2018wr023822

EURO-CORDEX. (2019). EURO-CORDEX data [Dataset]. Retrieved from https://esg-dn1.nsc.liu.se/search/cordex/

Eurostat. (2019). EUROPOP2019. *Population projections at regional level*, 2019–2100.

Ferguson, I. M., & Maxwell, R. M. (2010). Role of groundwater in watershed response and land surface feedbacks under climate change. *Water Resources Research*, *46*(10). https://doi.org/10.1029/2009wr008616

Forshay, K. J., & Stanley, E. H. (2005). Rapid nitrate loss and denitrification in a temperate river floodplain. *Biogeochemistry*, *75*(1), 43–64. https://doi.org/10.1007/s10533-004-6016-4

Garris, H. W., Mitchell, R. J., Fraser, L. H., & Barrett, L. R. (2014). Forecasting climate change impacts on the distribution of wetland habitat in the Midwestern United States. *Global Change Biology*, *21*(2), 766–776. https://doi.org/10.1111/gcb.12748

Gattringer, J. P., Maier, N., Breuer, L., Otte, A., Donath, T. W., Kraft, P., & Harvolk-Schöning, S. (2019). Modelling of rare flood meadow species distribution by a combined habitat surface water-groundwater model. *Ecohydrology*, *12*(6). https://doi.org/10.1002/eco.2122

Gelfan, A., Kalugin, A., Krylenko, I., Nasonova, O., Gusev, Y., & Kovalev, E. (2020). Does a successful comprehensive evaluation increase confidence in a hydrological model intended for climate impact assessment? *Climatic Change*, *163*(3), 1165–1185. https://doi.org/10.1007/s10584-020-02930-z

Giuntoli, I., Vidal, J.-P., Prudhomme, C., & Hannah, D. M. (2015). Future hydrological extremes: The uncertainty from multiple global climate and global hydrological models. *Earth System Dynamics*, *6*(1), 267–285. https://doi.org/10.5194/esd-6-267-2015

Glińska-Lewczuk, K., Burandt, P., Kujawa, R., Kobus, S., Obolewski, K., Dunalska, J., et al. (2016). Environmental factors structuring fish communities in floodplain lakes of the undisturbed system of the Biebrza River. *Water*, *8*(4), 146. https://doi.org/10.3390/w8040146

Goderniaux, P., Brouyère, S., Fowler, H. J., Blenkinsop, S., Therrien, R., Orban, P., & Dassargues, A. (2009). Large scale surface-subsurface hydrological model to assess climate change impacts on groundwater reserves. *Journal of Hydrology*, *373*(1–2), 122–138. https://doi.org/10.1016/j.jhydrol.2009.04.017

Goverment, Polish (2019). Open data portal [Dataset] in polish. https://dane.gov.pl/pl/dataset/2167,mapa-podzialu-hydrograficznego-polski-w-skali-110

Grabowska, M., Glińska-Lewczuk, K., Obolewski, K., Burandt, P., Kobus, S., Dunalska, J., et al. (2014). Effects of hydrological and physicochemical factors on phytoplankton communities in floodplain lakes. *Polish Journal of Environmental Studies*, *23*(3), 713–725.

Gramacy, R. B., & Taddy, M. (2010). Categorical inputs, sensitivity analysis, optimization and importance tempering with tgp version 2, an R package for treed Gaussian process models. *Journal of Statistical Software*, *33*(6), 1–48. https://doi.org/10.18637/jss.v033.i06

Grygoruk, M., Kochanek, K., & Mirosław-Świątek, D. (2021). Analysis of long-term changes in inundation characteristics of near-natural temperate riparian habitats in the lower basin of the Biebrza valley, Poland. *Journal of Hydrology: Regional Studies*, *36*, 100844. https://doi.org/10.1016/j.ejrh.2021.100844

Gudmundsson, L., Bremnes, J. B., Haugen, J. E., & Engen-Skaugen, T. (2012). Technical note: Downscaling RCM precipitation to the station scale using statistical transformation—A comparison of methods. *Hydrology and Earth System Sciences*, *16*(9), 3383–3390. https://doi.org/10.5194/hess-16-3383-2012

GUGiK. (2019). Polish geoportal [Dataset]. https://mapy.geoportal.gov.pl/imap/Imgp_2.html?gpmap=gp0

Hallberg, L., Hallin, S., & Bieroza, M. (2022). Catchment controls of denitrification and nitrous oxide production rates in headwater remediated agricultural streams. *Science of the Total Environment*, *838*, 156513. https://doi.org/10.1016/j.scitotenv.2022.156513

Hwang, H.-T., Park, Y.-J., Sudicky, E., & Forsyth, P. (2014). A parallel computational framework to solve flow and transport in integrated surface subsurface hydrologic systems. *Environmental Modelling & Software*, *61*, 39–58. https://doi.org/10.1016/j.envsoft.2014.06.024

Iribar, A., Hallin, S., Pérez, J. M. S., Enwall, K., Poulet, N., & Garabétian, F. (2015). Potential denitrification rates are spatially linked to colonization patterns of nosZ genotypes in an alluvial wetland. *Ecological Engineering*, *80*, 191–197. https://doi.org/10.1016/j.ecoleng.2015.02.002

Jacob, D., Petersen, J., Eggert, B., Alias, A., Christensen, O. B., Bouwer, L. M., et al. (2014). Euro-cordex: New high-resolution climate change projections for European impact research. *Regional Environmental Change*, *14*(2), 563–578. https://doi.org/10.1007/s10113-013-0499-2

Jacobson, R. B., Bouska, K. L., Bulliner, E. A., Lindner, G. A., & Paukert, C. P. (2022). Geomorphic controls on floodplain connectivity, ecosystem services, and sensitivity to climate change: An example from the lower Missouri River. *Water Resources Research*, *58*(6). https://doi.org/10.1029/2021wr031204

Joint Research Center. (2019). Agri4Cast resources portal [Dataset]. https://agri4cast.jrc.ec.europa.eu/dataportal/

Jones, C. N., Scott, D. T., Edwards, B. L., & Keim, R. F. (2014). Perirheic mixing and biogeochemical processing in flow-through and backwater floodplain wetlands. *Water Resources Research*, *50*(9), 7394–7405. https://doi.org/10.1002/2014wr015647

Kaser, D., Graf, T., Cochand, F., McLaren, R., Therrien, R., & Brunner, P. (2014). Channel representation in physically based models coupling groundwater and surface water: Pitfalls and how to avoid them. *Ground Water*, *52*(6), 827–836. https://doi.org/10.1111/gwat.12143

Keizer, F., der Lee, G. V., Schot, P., Kardel, I., Barendregt, A., & Wassen, M. (2018). Floodplain plant productivity is better predicted by particulate nutrients than by dissolved nutrients in floodwater. *Ecological Engineering*, *119*, 54–63. https://doi.org/10.1016/j.ecoleng.2018.05.024

Keizer, F., Schot, P., Okruszko, T., Chormanski, J., Kardel, I., & Wassen, M. (2014). A new look at the flood pulse concept: The (ir)relevance of the moving littoral in temperate zone rivers. *Ecological Engineering*, *64*(0), 85–99. https://doi.org/10.1016/j.ecoleng.2013.12.031

Kotowski, W., Jabłońska, E., & Bartoszuk, H. (2013). Conservation management in fens: Do large tracked mowers impact functional plant diversity? *Biological Conservation*, *167*, 292–297. https://doi.org/10.1016/j.biocon.2013.08.021

Kristensen, K. J., & Jensen, S. E. (1975). A model for estimating actual evapotranspiration from potential evapotranspiration. *Hydrology Research*, *6*(3), 170–188. https://doi.org/10.2166/nh.1975.0012

Krysanova, V., Donnelly, C., Gelfan, A., Gerten, D., Arheimer, B., Hattermann, F., & Kundzewicz, Z. W. (2018). How the performance of hydrological models relates to credibility of projections under climate change. *Hydrological Sciences Journal*, *63*(5), 696–720. https://doi.org/10.1080/02626667.2018.1446214

Kundzewicz, Z., Krysanova, V., Benestad, R., Hov, Ø., Piniewski, M., & Otto, I. (2018). Uncertainty in climate change impacts on water resources. *Environmental Science & Policy*, *79*, 1–8. https://doi.org/10.1016/j.envsci.2017.10.008

Laranjeiras, T. O., Naka, L. N., Leite, G. A., & Cohn-Haft, M. (2021). Effects of a major Amazonian river confluence on the distribution of floodplain forest avifauna. *Journal of Biogeography*, *48*(4), 847–860. https://doi.org/10.1111/jbi.14042

Lawler, J. J. (2009). Climate change adaptation strategies for resource management and conservation planning. *Annals of the New York Academy of Sciences*, *1162*(1), 79–98. https://doi.org/10.1111/j.1749-6632.2009.04147.x

Lew, S., Glińska-Lewczuk, K., Burandt, P., Obolewski, K., Goździejewska, A., Lew, M., & Dunalska, J. (2016). Impact of environmental factors on bacterial communities in floodplain lakes differed by hydrological connectivity. *Limnologica*, *58*, 20–29. https://doi.org/10.1016/j.limno.2016.02.005

McClain, M. E., Boyer, E. W., Dent, C. L., Gergel, S. E., Grimm, N. B., Groffman, P. M., et al. (2003). Biogeochemical hot spots and hot moments at the interface of terrestrial and aquatic ecosystems. *Ecosystems*, *6*(4), 301–312. https://doi.org/10.1007/s10021-003-0161-9

Mertes, L. A. K. (1997). Documentation and significance of the perirheic zone on inundated floodplains. *Water Resources Research*, *33*(7), 1749–1762. https://doi.org/10.1029/97wr00658

Moomaw, W. R., Chmura, G. L., Davies, G. T., Finlayson, C. M., Middleton, B. A., Natali, S. M., et al. (2018). Wetlands in a changing climate: Science, policy and management. *Wetlands*, *38*(2), 183–205. https://doi.org/10.1007/s13157-018-1023-8

Mosner, E., Weber, A., Carambia, M., Nilson, E., Schmitz, U., Zelle, B., et al. (2015). Climate change and floodplain vegetation - Future prospects for riparian habitat availability along the Rhine river. *Ecological Engineering*, *82*, 493–511. https://doi.org/10.1016/j.ecoleng.2015.05.013

Murray-Hudson, M., Wolski, P., & Ringrose, S. (2006). Scenarios of the impact of local and upstream changes in climate and water use on hydro-ecology in the Okavango Delta, Botswana. *Journal of Hydrology*, *331*(1–2), 73–84. https://doi.org/10.1016/j.jhydrol.2006.04.041

Natho, S., Tschikof, M., Bondar-Kunze, E., & Hein, T. (2020). Modeling the effect of enhanced lateral connectivity on nutrient retention capacity in large river floodplains: How much connected floodplain do we need? *Frontiers in Environmental Science*, *8*. https://doi.org/10.3389/fenvs.2020.00074

Nogueira, G. E. H., Schmidt, C., Partington, D., Brunner, P., & Fleckenstein, J. H. (2022). Spatiotemporal variations in water sources and mixing spots in a riparian zone. *Hydrology and Earth System Sciences*, *26*(7), 1883–1905. https://doi.org/10.5194/hess-26-1883-2022

O'Connor, B. L., Hondzo, M., Dobraca, D., LaPara, T. M., Finlay, J. C., & Brezonik, P. L. (2006). Quantity-activity relationship of denitrifying bacteria and environmental scaling in streams of a forested watershed. *Journal of Geophysical Research*, *111*(G4), G04014. https://doi.org/10.1029/2006jg000254

Pałczyński, A. (1984). Natural differentiation of plant communities in relation to hydrological conditions of the Biebrza valley. *Polish Ecological Studies*, *10*, 347–385.

Park, E., & Latrubesse, E. M. (2015). Surface water types and sediment distribution patterns at the confluence of mega Rivers: The Solimões-Amazon and Negro Rivers junction. *Water Resources Research*, *51*(8), 6197–6213. https://doi.org/10.1002/2014wr016757

Partington, D., Brunner, P., Simmons, C., Therrien, R., Werner, A., Dandy, G., & Maier, H. (2011). A hydraulic mixing-cell method to quantify the groundwater component of streamflow within spatially distributed fully integrated surface water-groundwater flow models. *Environmental Modelling & Software*, *26*(7), 886–898. https://doi.org/10.1016/j.envsoft.2011.02.007

Perra, E., Piras, M., Deidda, R., Paniconi, C., Mascaro, G., Vivoni, E. R., et al. (2018). Multimodel assessment of climate change-induced hydrologic impacts for a Mediterranean catchment. *Hydrology and Earth System Sciences*, *22*(7), 4125–4143. https://doi.org/10.5194/hess-22-4125-2018

Physical Sciences Laboratory. (2019). 20th century reanalysis (V3) data portal [Dataset]. https://psl.noaa.gov/data/gridded/data.20thC_ReanV3.html

Piniewski, M., Szcześniak, M., Kardel, I., Chattopadhyay, S., & Berezowski, T. (2021). G2dc-pl+: A gridded 2 km daily climate dataset for the union of the polish territory and the vistula and odra basins. *Earth System Science Data*, *13*(3), 1273–1288. https://doi.org/10.5194/essd-13-1273-2021

Polish Geological Institute. (2014). Central geological database [Dataset]. https://baza.pgi.gov.pl/geoportal/uslugi/gis

Politti, E., Egger, G., Angermann, K., Rivaes, R., Blamauer, B., Klösch, M., et al. (2014). Evaluating climate change impacts on Alpine floodplain vegetation. *Hydrobiologia*, *737*(1), 225–243. https://doi.org/10.1007/s10750-013-1801-5

Prudhomme, C., Giuntoli, I., Robinson, E. L., Clark, D. B., Arnell, N. W., Dankers, R., et al. (2013). Hydrological droughts in the 21st century, hotspots and uncertainties from a global multimodel ensemble experiment. *Proceedings of the National Academy of Sciences of the United States of America*, *111*(9), 3262–3267. https://doi.org/10.1073/pnas.1222473110

Racchetti, E., Bartoli, M., Soana, E., Longhi, D., Christian, R. R., Pinardi, M., & Viaroli, P. (2011). Influence of hydrological connectivity of riverine wetlands on nitrogen removal via denitrification. *Biogeochemistry*, *103*(1), 335–354. https://doi.org/10.1007/s10533-010-9477-7

Ramteke, G., Singh, R., & Chatterjee, C. (2020). Assessing impacts of conservation measures on watershed hydrology using MIKE SHE model in the face of climate change. *Water Resources Management*, *34*(13), 4233–4252. https://doi.org/10.1007/s11269-020-02669-3

Scaroni, A. E., Nyman, J. A., & Lindau, C. W. (2011). Comparison of denitrification characteristics among three habitat types of a large river floodplain: Atchafalaya River Basin, Louisiana. *Hydrobiologia*, *658*(1), 17–25. https://doi.org/10.1007/s10750-010-0471-9

Scott, D. T., Keim, R. F., Edwards, B. L., Jones, C. N., & Kroes, D. E. (2014). Floodplain biogeochemical processing of floodwaters in the Atchafalaya River basin during the Mississippi River flood of 2011. *Journal of Geophysical Research: Biogeosciences*, *119*(4), 537–546. 2013JG002477. https://doi.org/10.1002/2013jg002477

Sebben, M. L., Werner, A. D., Liggett, J. E., Partington, D., & Simmons, C. T. (2013). On the testing of fully integrated surface-subsurface hydrological models. *Hydrological Processes*, *27*(8), 1276–1285. https://doi.org/10.1002/hyp.9630

Shellberg, J. G., Brooks, A. P., Spencer, J., & Ward, D. (2013). The hydrogeomorphic influences on alluvial gully erosion along the Mitchell River fluvial megafan. *Hydrological Processes*, *27*(7), 1086–1104. https://doi.org/10.1002/hyp.9240

Shewchuk, J. (1996). Triangle: Engineering a 2d quality mesh generator and delaunay triangulator. In M. Lin & D. Manocha (Eds.), *Lecture notes in computer science* (Vol. 1148, pp. 203–222). Springer Berlin Heidelberg.

Slater, L. J., Khouakhi, A., & Wilby, R. L. (2019). River channel conveyance capacity adjusts to modes of climate variability. *Scientific Reports*, *9*(1), 12619. https://doi.org/10.1038/s41598-019-48782-1

Slater, L. J., & Singer, M. B. (2013). Imprint of climate and climate change in alluvial riverbeds: Continental United States, 1950-2011. *Geology*, *41*(5), 595–598. https://doi.org/10.1130/g34070.1

Slivinski, L. C., Compo, G. P., Whitaker, J. S., Sardeshmukh, P. D., Giese, B. S., McColl, C., et al. (2019). Towards a more reliable historical reanalysis: Improvements for version 3 of the Twentieth Century Reanalysis system. *Quarterly Journal of the Royal Meteorological Society*, *145*(724), 2876–2908. https://doi.org/10.1002/qj.3598

Słowik, M. (2022). The evolution of meandering and Anabranching Rivers in postglacial and loess landscapes of Europe. *The Holocene*, *33*(2), 208–230. https://doi.org/10.1177/09596836221131712

Statistics Poland. (2021). Population by sex, feminization rate, population density. *Teritorial units: Podlaskie and Warminsko-Mazurskie*. Retrieved from swaid.stat.gov.pl

Sulis, M., Paniconi, C., Marrocu, M., Huard, D., & Chaumont, D. (2012). Hydrologic response to multimodel climate output using a physically based model of groundwater/surface water interactions. *Water Resources Research*, *48*(12). https://doi.org/10.1029/2012wr012304

Sulis, M., Paniconi, C., Rivard, C., Harvey, R., & Chaumont, D. (2011). Assessment of climate change impacts at the catchment scale with a detailed hydrological model of surface-subsurface interactions and comparison with a land surface model. *Water Resources Research*, *47*(1). https://doi.org/10.1029/2010wr009167

Thompson, J. R., Crawley, A., & Kingston, D. G. (2016). GCM-Related uncertainty for river flows and inundation under climate change: The inner Niger delta. *Hydrological Sciences Journal*, *61*(13), 2325–2347. https://doi.org/10.1080/02626667.2015.1117173

Tomasek, A., Kozarek, J. L., Hondzo, M., Lurndahl, N., Sadowsky, M. J., Wang, P., & Staley, C. (2017). Environmental drivers of denitrification rates and denitrifying gene abundances in channels and riparian areas. *Water Resources Research*, *53*(8), 6523–6538. https://doi.org/10.1002/2016wr019566

van Loon, A., Schot, P., Griffioen, J., Bierkens, M., Batelaan, O., & Wassen, M. (2009). Throughflow as a determining factor for habitat contiguity in a near-natural fen. *Journal of Hydrology*, *379*(1–2), 30–40. https://doi.org/10.1016/j.jhydrol.2009.09.041

Veijalainen, N., Lotsari, E., Alho, P., Vehviläinen, B., & Käyhkö, J. (2010). National scale assessment of climate change impacts on flooding in Finland. *Journal of Hydrology*, *391*(3–4), 333–350. https://doi.org/10.1016/j.jhydrol.2010.07.035

Wassen, M. J., Okruszko, T., Kardel, I., Chormanski, J., Swiatek, D., Mioduszewski, W., et al. (2006). Eco-hydrological functioning of the biebrza wetlands: Lessons for the conservation and restoration of deteriorated wetlands rid c-7306-2008. Wetlands: Functioning. *Biodiversity Conservation, and Restoration*, *191*, 285–310.

Wen, L., Macdonald, R., Morrison, T., Hameed, T., Saintilan, N., & Ling, J. (2013). From hydrodynamic to hydrological modelling: Investigating long-term hydrological regimes of key wetlands in the Macquarie Marshes, a semi-arid lowland floodplain in Australia. *Journal of Hydrology*, *500*, 45–61. https://doi.org/10.1016/j.jhydrol.2013.07.015

Yuan, X., Lu, Y., Jiang, L., Liang, S., Jiang, Y., & Xiao, F. (2021). Runoff responses to climate change in China's Buyuan River basin. *River Research and Applications*, *37*(8), 1134–1144. https://doi.org/10.1002/rra.3785

Zulkafli, Z., Buytaert, W., Manz, B., Rosas, C. V., Willems, P., Lavado-Casimiro, W., et al. (2016). Projected increases in the annual flood pulse of the Western Amazon. *Environmental Research Letters*, *11*(1), 014013. https://doi.org/10.1088/1748-9326/11/1/014013

References From the Supporting Information

Alfieri, L., Burek, P., Feyen, L., & Forzieri, G. (2015). Global warming increases the frequency of river floods in Europe. *Hydrology and Earth System Sciences*, *19*(5), 2247–2260. https://doi.org/10.5194/hess-19-2247-2015

Anonymous (1912). *Summary of water levels on the inland water ways of Russia from observations at water gauge posts. Period: 1881-1910*. Ministry of Communications, Internal Control, Waterways, and Roads.

Anonymous (1932). *Hydrographic yearbook. Vistula basin. Period: 1918-1932*. Ministerstwo komunikacji.

Berezowski, T. (2023). Hydrological indicators of water zones in inundation, historical water levels, and forcing data for the 1881-2099 [Dataset]. Period in the lower biebrza valley. https://doi.org/10.34808/323p-nd55

Berezowski, T., Szcześniak, M., Kardel, I., Michałowski, R., Okruszko, T., Mezghani, A., & Piniewski, M. (2016). Cplfd-gdpt5: High-resolution gridded daily precipitation and temperature data set for two largest polish river basins. *Earth System Science Data*, *8*(1), 127–139. https://doi.org/10.5194/essd-8-127-2016

Chen, J., Sudicky, E. A., Davison, J. H., Frey, S. K., Park, Y.-J., Hwang, H.-T., et al. (2019). Towards a climate-driven simulation of coupled surface-subsurface hydrology at the continental scale: A Canadian example. *Canadian Water Resources Journal/Revue canadienne des ressources hydriques*, *45*(1), 11–27. https://doi.org/10.1080/07011784.2019.1671235

Chow, V. T., Maidment, D., & Mays, L. (1988). Applied hydrology. *McGraw-Hill*.

Doncker, L. D., Troch, P., Verhoeven, R., Bal, K., Meire, P., & Quintelier, J. (2009). Determination of the Manning roughness coefficient influenced by vegetation in the river Aa and Biebrza river. *Environmental Fluid Mechanics*, *9*(5), 549–567. https://doi.org/10.1007/s10652-009-9149-0

Dąbrowska-Zielińska, K., Budzyńska, M., Tomaszewska, M., Bartold, M., Gatkowska, M., Malek, I., et al. (2014). Monitoring wetlands ecosystems using ALOS PALSAR (L-band, HV) supplemented by optical data: A case study of Biebrza wetlands in northeast Poland. *Remote Sensing*, *6*(2), 1605–1633. https://doi.org/10.3390/rs6021605

Gnatowski, T., Szatyłowicz, J., Brandyk, T., & Kechavarzi, C. (2010). Hydraulic properties of fen peat soils in Poland. *Geoderma*, *154*(3–4), 188–195. https://doi.org/10.1016/j.geoderma.2009.02.021

Kundzewicz, Z. W., Krysanova, V., Dankers, R., Hirabayashi, Y., Kanae, S., Hattermann, F. F., et al. (2016). Differences in flood hazard projections in Europe - Their causes and consequences for decision making. *Hydrological Sciences Journal*, 02626667.2016.1241398. https://doi.org/10.1080/02626667.2016.1241398

Marx, A., Kumar, R., Thober, S., Rakovec, O., Wanders, N., Zink, M., et al. (2018). Climate change alters low flows in Europe under global warming of 1.5, 2, and 3c. *Hydrology and Earth System Sciences*, *22*(2), 1017–1032. https://doi.org/10.5194/hess-22-1017-2018

Meresa, H., Osuch, M., & Romanowicz, R. (2016). Hydro-meteorological drought projections into the 21-st century for selected Polish catchments. *Water*, *8*(5), 206. https://doi.org/10.3390/w8050206

Mezghani, A., Dobler, A., Haugen, J. E., Benestad, R. E., Parding, K. M., Piniewski, M., et al. (2017). CHASE-PL climate projection dataset over Poland - Bias adjustment of EURO-CORDEX simulations. *Earth System Science Data*, *9*(2), 905–925. https://doi.org/10.5194/essd-9-905-2017

Osuch, M., Lawrence, D., Meresa, H. K., Napiorkowski, J. J., & Romanowicz, R. J. (2016). Projected changes in flood indices in selected catchments in Poland in the 21st century. *Stochastic Environmental Research and Risk Assessment*, *31*(9), 2435–2457. https://doi.org/10.1007/s00477-016-1296-5

Piniewski, M., Szcześniak, M., Kundzewicz, Z. W., Mezghani, A., & Hov, Ø. (2017). Changes in low and high flows in the Vistula and the Odra basins: Model projections in the European-scale context. *Hydrological Processes*, *31*(12), 2210–2225. https://doi.org/10.1002/hyp.11176

Rawson, H. M., & Macpherson, H. G. (2000). Irrigated wheat. *FAO*. www.fao.org/3/X8234E/X8234E00.html

Roudier, P., Andersson, J. C. M., Donnelly, C., Feyen, L., Greuell, W., & Ludwig, F. (2015). Projections of future floods and hydrological droughts in Europe under a +2c global warming. *Climatic Change*, *135*(2), 341–355. https://doi.org/10.1007/s10584-015-1570-4

Schneider, C., Laizé, C. L. R., Acreman, M. C., & Flörke, M. (2013). How will climate change modify river flow regimes in Europe? *Hydrology and Earth System Sciences*, *17*(1), 325–339. https://doi.org/10.5194/hess-17-325-2013

Świątek, D., & Okruszko, T. (2003). Analysis of impact of natural stream bed variability representation on computed water surface. *Wethydro - workshop 1*. http://levis.sggw.waw.pl/wethydro/contents/monografie/ws1/117-126SwiatekOkruszko_e.pdf

Suliga, J., Chormański, J., Szporak-Wasilewska, S., Kleniewska, M., Berezowski, T., van Griensven, A., & Verbeiren, B. (2015). Derivation from the Landsat 7 NDVI and ground truth validation of LAI and interception storage capacity for wetland ecosystems in Biebrza Valley, Poland. In C. M. U. Neale & A. Maltese (Eds.), *Remote sensing for agriculture, ecosystems, and hydrology XVII* (Vol. 9637, p. 96371Z). SPIE. https://doi.org/10.1117/12.2194975

Warszawski, L., Frieler, K., Huber, V., Piontek, F., Serdeczny, O., & Schewe, J. (2013). The inter-sectoral impact model intercomparison project (ISI-MIP): Project framework. *Proceedings of the National Academy of Sciences of the United States of America*, *111*(9), 3228–3232. https://doi.org/10.1073/pnas.1312330110

Wösten, J., Lilly, A., Nemes, A., & Bas, C. L. (1999). Development and use of a database of hydraulic properties of European soils. *Geoderma*, *90*(3–4), 169–185. https://doi.org/10.1016/s0016-7061(98)00132-3